STRUCTURAL BEHAVIOR OF HYBRID FIBER REINFORCED CONCRETE PANELS UNDER BLAST LOADS

A Thesis Submitted to
the Graduate School of Engineering and Sciences of
İzmir Institute of Technology
In Partial Fulfillment of the Requirements for the Degree of

MASTER OF SCIENCE

in Civil Engineering

by
Mouhammed Jalal ALKABBANI

July 2021
İZMİR

ACKNOWLEDGMENTS

I would like to express my deepest appreciation to my supervisor Assist. Prof. Dr.Selçuk Saatcı for giving me the chance to join this precious project, his keen guidance, and making me capable of conducting independent research. Without his continuous support and patience, it would be an enormous task. I also owe to Assoc. Prof. Dr. Tahir Kemal Erdem for helping and guiding me in the concrete mix design and casting process.

Besides my advisor, I am grateful to Cemal Kılıç, Structural Mechanics Laboratory Technician, for his help and guidance which was essential in facilitating and carrying out the experimental work. I would also thank my colleagues and friends in the university and outside the University for their support and encouragement.

This study was funded by the Scientific and Technological Research Council of Turkey, TUBITAK under 217M442.

Many thanks to Türkiye Bursları Scholarship, which sponsored my arrival to Turkey and the pursuit of my master's degree.

I would love to thank my family, Amira Salamah and Muhammed Arif for their continuous support.

Lastly, I would love to thank my parents, Muhammed Aref Alkabbani and Maha Salamah, and my brothers, for their continuous support.

ABSTRACT

STRUCTURAL BEHAVIOR OF HYBRID FIBER REINFORCED CONCRETE PANELS UNDER BLAST LOADS

Terrorist attacks cause injuries and casualties not only due to direct effect of explosions, but also due to collapse of non-structural elements in buildings such as brick walls. Strengthening of non-blast resistant buildings to blast loads can be done using blast resistant cladding. In this study, structural behavior of panels manufactured using hybrid fiber reinforced concrete, composed of steel and synthetic polyvinyl alcohol (PVA) fibers, under blast loads was investigated and the potential use of such panels for the strengthening of existing buildings against blast loads was examined. For this purpose, 11 panels with 1900x1900x50 dimensions were tested under blast loads. Blast loads were applied on panels by a shock tube designed and manufactured within this project. As a result of the study, it was found that panels manufactured using hybrid fiber reinforced concrete had higher strength and energy absorption capacity under blast loads compared to panels manufactured by using steel fibers only. Using steel and PVA fibers provided a better control of micro and macro cracking and increased the panels' ductility. The study showed that hybrid fiber reinforced concrete panels can be used as a protective cladding for blast loads.

Keywords: Fiber Reinforced Concrete, Hybrid Fiber Reinforced Concrete, Cladding Panels, Blast Behavior of Structures, Blast Safety.

ÖZET

HİBRİT FİBERLİ BETON PANELLERİN PATLAMA YÜKÜ ALTINDA YAPISAL DAVRANIŞLARI

Terörist saldırılar sadece patlamaların doğrudan etkileri nedeniyle değil, aynı zamanda binalardaki tuğla duvar gibi yapısal olmayan elemanların çökmesiyle de can kaybına yol açmaktadır. Patlamalara karşı tasarlanmamış binaların patlama yüklerine karşı güçlendirilmesi patlamalara dayanıklı cephe kaplamalarıyla yapılabilir. Bu çalışmada çelik ve sentetik polivinil alkol (PVA) fiberlerden oluşan hibrit fiberli betondan imal edilen panellerin patlama yükleri karşısında yapısal davranışları incelenmiş ve bu panellerin mevcut binaların patlama yüklerine karşı güçlendirilmesi amacıyla kullanım potansiyelleri araştırılmıştır. Bu amaçla 1900x1900x50 mm boyutlarında 11 panel patlama yükleri altında test edilmiştir. Paneller üzerinde patlama yükleri bu proje kapsamında tasarlanan ve imal edilen bir şok tüpü vasıtasıyla uygulanmıştır. Çalışmanın sonucunda patlama yükleri altında hibrit fiberli betondan üretilen panellerin sadece çelik fiber kullanılan panellere göre daha yüksek dayanım ve enerji sönümleme kapasitesine sahip oldukları görülmüştür. Çelik ve PVA fiberlerin birlikte kullanımı mikro ve makro çatlakların daha iyi kontrolünü sağlamış ve panellerin sünekliğini arttırmıştır. Çalışma hibrit fiberli beton panellerin patlama yüklerine karşı koruyucu cephe kaplaması olarak kullanılabileceğini göstermiştir.

Anahtar Kelimeler: Fiberli Beton, Hibrit Fiberli Beton, Cephe Kaplama Panelleri, Yapıların Patlama Davranışı, Patlama Güvenliği.

TABLE OF CONTENTS

LIST OF FIGURES

Figure **Page**

Figure **Page**

Figure **Page**

LIST OF TABLES

CHAPTER 1

INTRODUCTION

In recent decades, terrorist attacks such as bombings are increased to target not just military buildings but also civilian structures (Figure 1.1). Explosives directed towards vulnerable structures may cause considerable damage and loss of life. In these explosions, exterior brick walls which are directly exposed to the shock wave could collapse completely and injure the people inside. Moreover, the building becomes unusable beyond repair. However, in such events, most of the damage occurs in non-load-bearing components instead of structural components such as columns.

(a) Diyarbakir Cinar District Police Department (14.01.2016)

(b) Mardin Midyat District Police Department (08.06.2016)

Figure 1.1. Reinforced Concrete Buildings After Attacks With Explosive-Laden Vehicles

Strengthening of buildings that were not originally designed to be blast resistant can be done by using aluminum or reinforced concrete cladding. However, aluminum claddings are rather an expensive solution, whereas thick reinforced concrete claddings bring significant loads to the structure.

In this study, structural behavior of panels manufactured using hybrid fiber reinforced concrete, a recently developed concrete composed of steel and synthetic fibers, under blast loads were investigated and the potential use of such panels for the strengthening of existing buildings against blast loads was examined. Hybrid fiber reinforced concrete is a composite material that exhibits strain hardening behavior under flexure and it is more ductile compared to normal, steel fiber or synthetic fiber reinforced concrete. Due this property, it can be considered to have a high potential to dissipate blast load energy, which is the main hypothesis of the study. There are no available studies in the literature about the structural behavior of hybrid fiber reinforced concrete panels under blast loads. This study aimed to fill this gap in this area.

The study presented here involves an experimental investigation of the structural behavior of hybrid fiber reinforced concrete (HyFRC) panels with respect to varying steel and poly vinyl alcohol (PVA) fiber contents. Including three trial specimens, a total of 16 panels were cast and tested under impulsive loads. To simulate the blast load in a laboratory environment, a shock tube was designed and manufactured. By means of this shock tube, an impulsive load that mimics a typical blast load was created by the sudden release of compressed air. Specimens tested with this shock tube were examined and their behavior was compared.

CHAPTER 2

LITERATURE REVIEW

An explosion is a rapid release of energy caused by a very fast chemical reaction. As a result, highly compressed air travels from the source in a hemispherical wave propagation and hits the target. This wave is called a shock wave (Institution of Civil Engineers, 1995). The hemispherical shock wave creates an instantaneous higher positive blast pressure on the structure in the direction of the wave. When the blast wave transits away from the point of detonation, the blast pressure reflects causing a negative suction phase. As the blast wave continues to propagate, energy loss occurs and the blast pressure decreases to ambient atmospheric pressure.

The maximum blast pressure is directly proportional to the mass of the explosive material and inversely related to its distance. Because the blast pressure generally affects the structures in much shorter times compared to their natural vibration period, the destructive effect on the structure comes from the total impulse created by the explosion pressure, not from the maximum pressure (Chopra, 1995). Therefore, in blast-resistance structure designs, the ductility of the structure is as important as its strength.

The design of buildings against accidental explosions is a subject that has been studied for many years, especially by military units. There are many standards published on the design of both architectural and structural systems of buildings against explosion loads (UFC 3-340-02, 2008; FEMA 426, 2003; ACI 370R-14, 2014). Application of blast-resistant cladding on the facade of buildings may provide blast resistance (Oswald ve Moriarty, 2014). Materials such as aluminum foam or honeycomb structures have high energy absorbing ability and are used as facade cladding to increase blast-resistant properties. However, covering large buildings with these materials has been a very expensive solution (Wu et al., 2011). For this reason, concrete-based coatings are more preferred despite the disadvantage of heaviness (Oswald and Bazand, 2014; Bewick et al., 2008). However, due to its low tensile strength, concrete is brittle and absorbs low energy. For these reasons, it was deemed necessary to apply various strengthening methods for reinforced concrete panels produced for blast-resistance. For example, one of the solutions was wrapping reinforced concrete panels with carbon or glass fiber

composite fabrics (Razaqpur vd., 2007; Razaqpur vd., 2009; Carriere vd., 2009; Tanapornraweekit vd., 2011). However, shear failures are common problems in such panels at supports points. In addition, debonding failures may also occur (Figure 2.1).

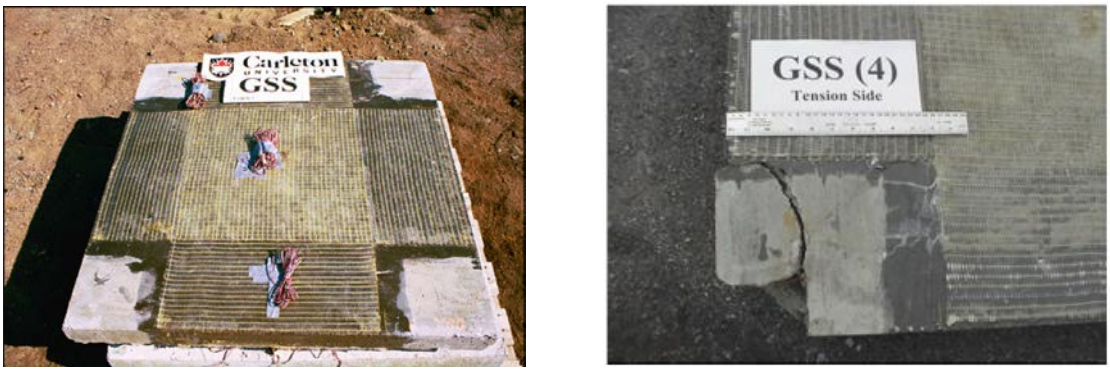

(a) Panel sample (b) Slip crack at supports

Figure 2.1. Explosion Behavior of Concrete Panels Covered With Glass Fiber Fabric (GFRP) (Source: Razaqpur et al, 2007)

Using varying fibers in the concrete mix increases the tensile strength of concrete that leads to an increase in the blast resistance (Cadoni et al., 2015; Enfedaque et al., 2011; Foglar and Kovar, 2014; Millard et al. , 2010). Steel or synthetic (polyvinyl alcohol (PVA), polyethylene, etc.) fibers used in the concrete mixture delay the opening of cracks that develop under load in the concrete and increase the tensile strength of the concrete, especially after cracking. The fibers in cracked concrete continue carrying the tensile stresses, which significantly increases the ductility of fiber reinforced concrete. This type of concrete is very suitable for situations where high energy absorption is required, such as impact and blast loads (Drdlova et al., 2015). A study performed by Tadepalli et al. (2009) concluded that the most effective steel fibers for improved energy absorption capacity and mechanical properties were hooked fibers.

In a previous project supported by TÜBİTAK (112M822), steel fiber reinforced concrete slabs and beams were tested under impact loads and it was observed that the specimens with fibers showed much higher impact resistance than those without fiber. Drop weights of the impact tests varied according to specimen, whereas the height of the free fall was fixed at 2.5 m, resulting 7.0 m/s contact velocity at the instant of impact. Both samples had same properties and ratio of reinforcement, but the difference was the

addition of 0.5% fiber of the volume to concrete. The specimen with fibers was tested once with 320 kg mass and twice with 555 kg on the midpoint of the slabs. Although the total impact energy received is much higher, the level of damage was slight. On the other hand, the specimen without fibers was tested once with 210 kg mass and twice with 320 kg, which created (Figure 2.2). The transfer of the tensile stresses between the crack surfaces was provided by the steel fibers. The absorption of the impact energy and ductility of the specimens significantly increased by using steel fibers. The shear strength also was increased in the specimen by adding steel fibers and the shrapnel effect was avoided by preventing the concrete pieces separating from the back surface.

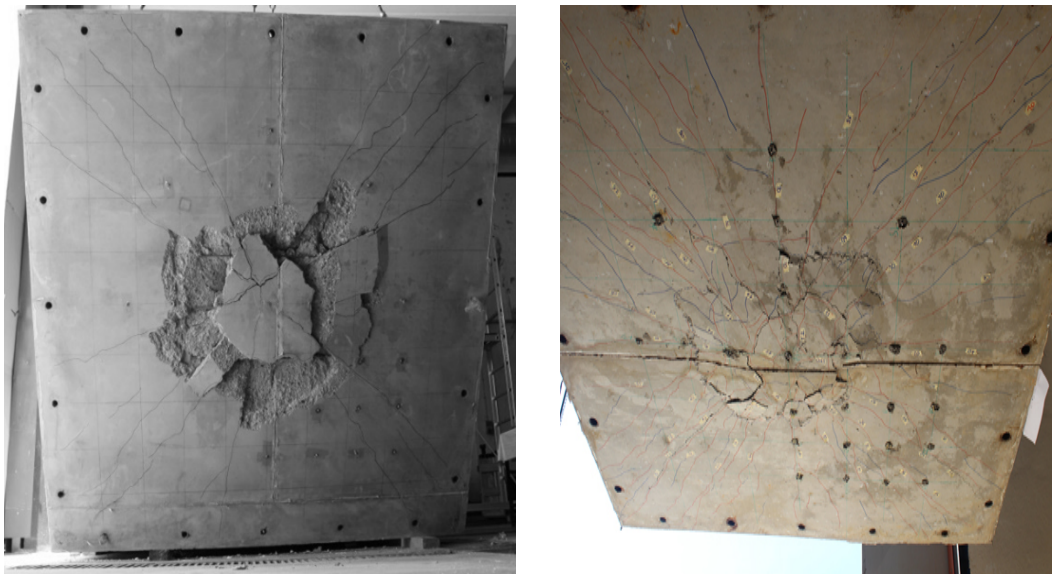

(a) Specimen without any fibers (b) Specimen with 0.5 % of steel fibers

Figure 2.2. Slabs With and Without Fibers After Impact Tests

A study carried out by Yusof et al. (2010) investigated the behavior of steel fiber reinforced concrete panels subjected to blast loading. A total of eight specimens of 600 mm x 600 mm x100 mm with 20 mm cover were cast and tested, including one normal reinforced concrete and seven variety volume fraction 0.5%, 1.0%, and 1.5% of hooked-end steel fiber. The panels were exposed to a blast shock wave generated by the detonation of 1kg of explosive charge located at a 0.6m standoff distance. The results showed that when the volume of fibers increased in panels the failure modes changed from brittle manner to pseudo-plastic manner and the damage classification varied from

severe to light. For example, the concrete which contains 0% and 0.5% of steel fibers shows flexural shear mode failure after testing. However, the panels containing 1% and 1.5% of steel fibers volume fraction of fibers show significant strength to resist the blast loading. The best behavior against blast loading was of the panels consisting of 1.5% of steel. Back and side face of panels after testing with the varying volume of steel fibers is shown in Figure 2.3.

Figure 2.3. Back and Side Face of Panels After Testing With the Varying Volume of Steel Fibers

A long steel fiber with high elastic modulus, tensile strength, and stiffness prevents the opening of macrocracks. On the other hand, short synthetic fibers with lower elastic modulus and tensile strength delay the development of microcracks (Betterman et al., 1995). Cement-based composites (engineered cementitious composite, ECC) developed using short synthetic fibers are a material that can achieve high deformations by showing strain hardening under axial stress (Şahmaran and Yaman, 2007). However, short synthetic fibers, which significantly improve the cracking resistance and post-cracking ductility of concrete, lose their effectiveness with the increase in crack width (Figure 2.4). There is no significant contribution of long steel fibers in carrying tensile forces before formation macrocracks, but this role can be taken more effectively after the development of wide cracks.

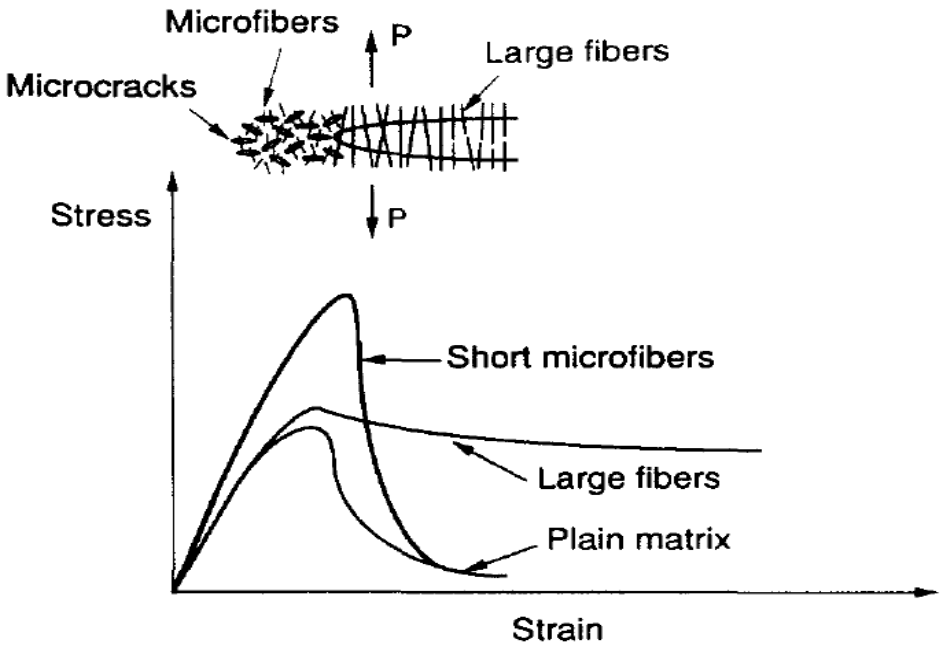

Figure 2.4. Effect of Fiber Size on Crack Bridging
(Source: Betterman et al., 1995)

In recent years, new concrete types have started to come to the fore, to benefit from the advantages of different types of fiber. When two or more types of fibers are incorporated in the same mix, resulting concrete is called hybrid fiber reinforced concrete (HyFRC). Steel and poly-vinyl alcohol (PVA) fibers are used extensively in many structures that require higher ductility, toughness, strength, energy absorption, and post cracking strength (Tadepalli et al., 2009). In hybrid fiber reinforced concrete, the coalescence of microcracks at an early stage are arrested by the synthetic fibers, conditionally leading to strength increase, while steel fibers later help increase the post-cracking toughness by effectively bridging the macrocracks on the surface (Chasioti and Vecchio, 2017; Abadel et al., 2017). In HyFRC, load-deflection curves, deformation hardening, and flexural tensile strength are significantly higher than the corresponding typical values for plain concrete. A project supported by TÜBİTAK (115M296) investigated the mechanical properties of and behavior of HyFRC under dynamic and impact tests. In this project, 38 different concrete mixtures were produced by using three different steel fiber types and synthetic (PVA) fibers in varying proportions. The beam specimens generating from these mixtures were cast and tested under static loads. In addition, six different mixtures were selected according to the best performance under static loads and the beam samples produced from these mixtures were tested under impact

loads. The properties of the selected mixtures are given in Table 2.1, and the static load-deflection curves obtained from four-point bending tests of 600x150x150 mm beams are given in Figure 2.5. The compressive strengths of selected mixes were between 35 and 40 MPa. As seen in Figure 2.5, the flexural strength and ductility of HyFRC samples were very high compared to plain concrete samples. A similar performance was observed in the impact tests. HyFRC specimens showed higher flexural strength, toughness and impact resistance. Impact test were made by dropping a 4.26 kg weight from 2 m height resulting in a speed of 6.3 m/s. The flexural strength (maximum tensile stress) and toughness obtained from the area under load-deflection curves were found for 600x100x100 mm beams and results are given in Table 2.2. The performance improvement in HyFRC was clearly seen.

Table 2.1. HyFRC Mixture Content

Mixture	Steel Fiber Types	Volume Fraction of Steel Fiber ,%	Volume Fraction of PVA , %	Aggregate Dmax (mm)
ST1,0.75_P0.25_D16	Dramix 30/40 3D	0.75	0.25	16
ST2,0.75_P0.25_D16	Dramix 65/60 3D	0.75	0.25	16
ST3,0.75_P0.25_D16	Dramix 65/60 5D	0.75	0.25	16
ST2,1.25_P0.25_D16	Dramix 65/60 3D	1.25	0.25	16
ST2,1.25_P0.25_D8	Dramix 65/60 3D	1.25	0.25	8
ST3,0.75_P.25_Per20_D16	Dramix 65/60 5D	0.75	0.25	16 (%20 perlite)

Table 2.2. Impact Loading Test Results

Mix	Flexural Strength (MPa)	Toughness (joule)
ST1,0.75_P0.25_D16	12,2	31,1
ST2,0.75_P0.25_D16	17,2	45,2
ST3,0.75_P0.25_D16	26,3	62,0
ST2,1.25_P0.25_D16	29,6	63,2
ST2,1.25_P0.25_D8	24,7	57,5
ST3,0.75_P.25_Per20_D16	18,6	43,5

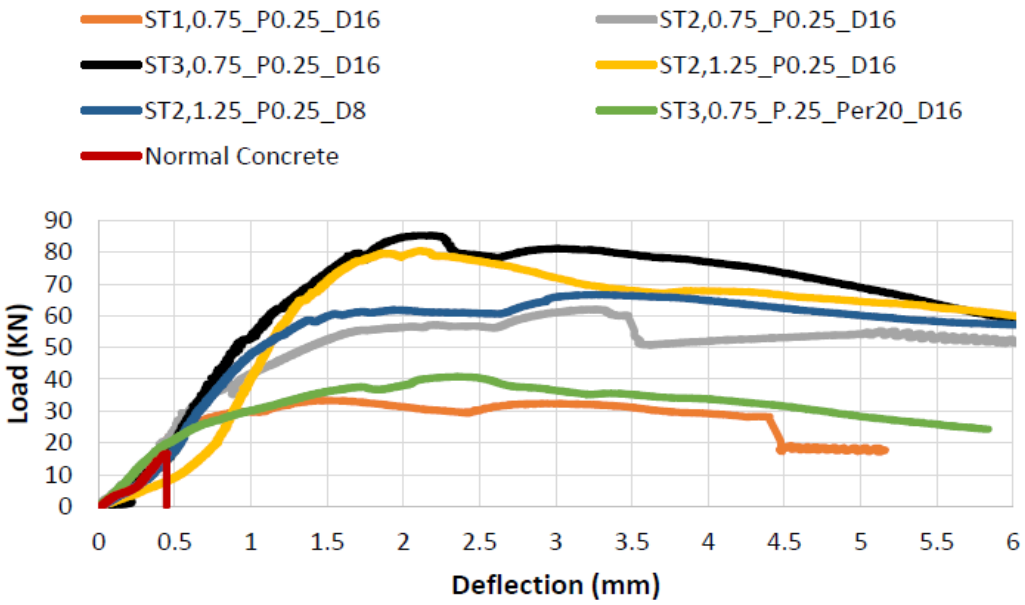

Figure 2.5. Load-Deflection Curves for HFRC

There are various researches on the behavior of steel or synthetic fiber concrete panels under blast loads, and their examination is quite extensive in the literature. Most of the experimental programs were concentrated on the craters and holes on the panels that were created after very close range or indirect contact explosion (Lan et al., 2005; Wang et al., 2013; Yamaguchi et al., 2011; Castedo et al., 2015; Yoo and Banthia, 2017). Experimental studies on the structural behavior of fiber reinforced concrete panels under blast load are quite limited (Li et al., 2015; Mao et al., 2014). The main reasons for this can be attributed to the difficulty of explosion tests, the necessity of taking numerous measurements in experiments focusing on structural behavior and the difficulties in terms of safety of the devices in explosion tests performed in the open field. To properly investigate the structural behavior, the specimens need to have dimensions close to the actual dimensions and to be properly supported in the experiments. For this reason, the structural behavior of panels under extreme loads such as blast loads is examined either by numerical studies (Haido et al., 2011; Zhou et al., 2014) or by impact tests (Zhang et al., 2007) as it is easier. However, complete information about the structural explosion load behavior is not given according to impact tests as it causes local effects such as crushing and punching. In this study, it was aimed to investigate the structural behavior of HyFRC panels under blast loads in a laboratory environment and fulfill a gap in the literature in this area.

CHAPTER 3

EXPERIMENTAL PROGRAM

3.1. General Information

The experimental study consisted of designing, constructing, and testing of thirteen thin panels, cast with steel fiber reinforced concrete (SFRC) and hybrid fiber reinforced concrete (HyFRC), with or without steel reinforcement. This program aimed to understand the structural behavior of the fiber reinforced concrete panels under blast loading and to see the effect of using steel and PVA fibers in the concrete panels on increasing their blast resistance.

A shock tube was used to simulate the blast wave on these specimens. Test specimens, material properties, test setup, instrumentation and test procedure were described in the following chapter.

3.2. Test specimens

In total, the experimental program was consisted of sixteen panels, which can be grouped as preliminary specimens and main specimens. Three preliminary specimens were used to test the shock tube, determine the testing conditions (level of pressure to be applied) and decide the thickness of the main panel specimens. Two of the preliminary panel specimens were cast with SFRC with dimensions of 1900x1900x50 mm and 1900x1900x75 mm. One preliminary specimen was designed to be a reinforced concrete (RC) rigid panel with dimensions of 1900x1900x100 mm. Reinforcement was placed in this specimen in a mesh form of 10 mm diameter deformed bars with 100 mm spacing in both orthogonal directions. Reinforcement mesh was placed close to the tension face of the panel with a clear cover of 20 mm (Figure 3.1).

Thirteen main specimens were cast with dimensions of 1900x1900x50 mm. The panels were cast in five pairs. Four of these pairs were without ordinary steel reinforcement and in every pair, one specimen was cast just with steel fiber and the other with steel and PVA fibers. The difference between four pairs was in the ratio of and type

of steel fibers. The fifth pair was cast with ordinary steel reinforcement and steel fibers, one with and one without PVA fibers. Steel reinforcement in these panels were in welded mesh form, with 5 mm steel bar diameter 150 mm spacing in both orthogonal directions. This reinforcement provided an equal reinforcement ratio of 0.45% in both directions. A clear cover of 20 mm from the tension face of the panel was provided (Figure 3.2).

Two panels were cast as reference specimens. One was cast as plain concrete (without any fibers and reinforcement), and the other with only steel reinforcement. In addition, one specimen with steel and PVA fibers was cast by replacing 20% of the volume of fine aggregate with lightweight perlite.

For casting the specimens, two formworks were designed and built from timber and plywood in the Structural Mechanics Laboratory at the Izmir Institute of Technology (IYTE) (See Figure 3.3). To make mounting of specimens to the shock tube easier, twelve 40 mm diameter of circular pieces wood were fixed in the wooden mold. Then, 50 mm long steel pipes installed on them to make holes during casting of panels. Pipes at each side were interconnected together by two welded steel bars on the sides to make them stay vertically during the casting. In addition, to lift, transport, and fix the specimens to the test setup, six U-shaped steel hooks were made. Four of these hooks were placed at suitable locations on the surface of the panel, and two were put laterally at one side.

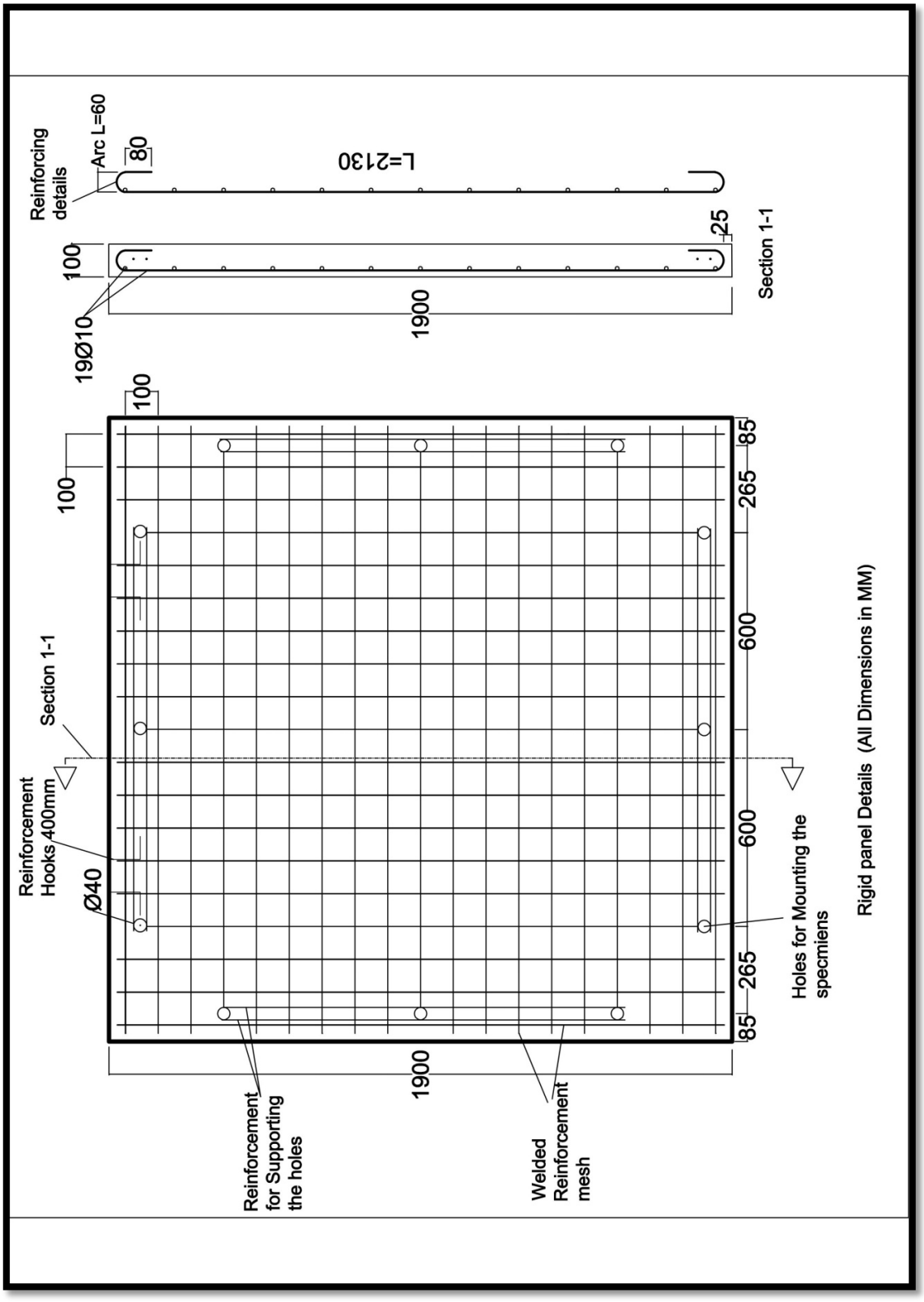

Figure 3.1. Rigid Panel Details (All Dimensions in mm)

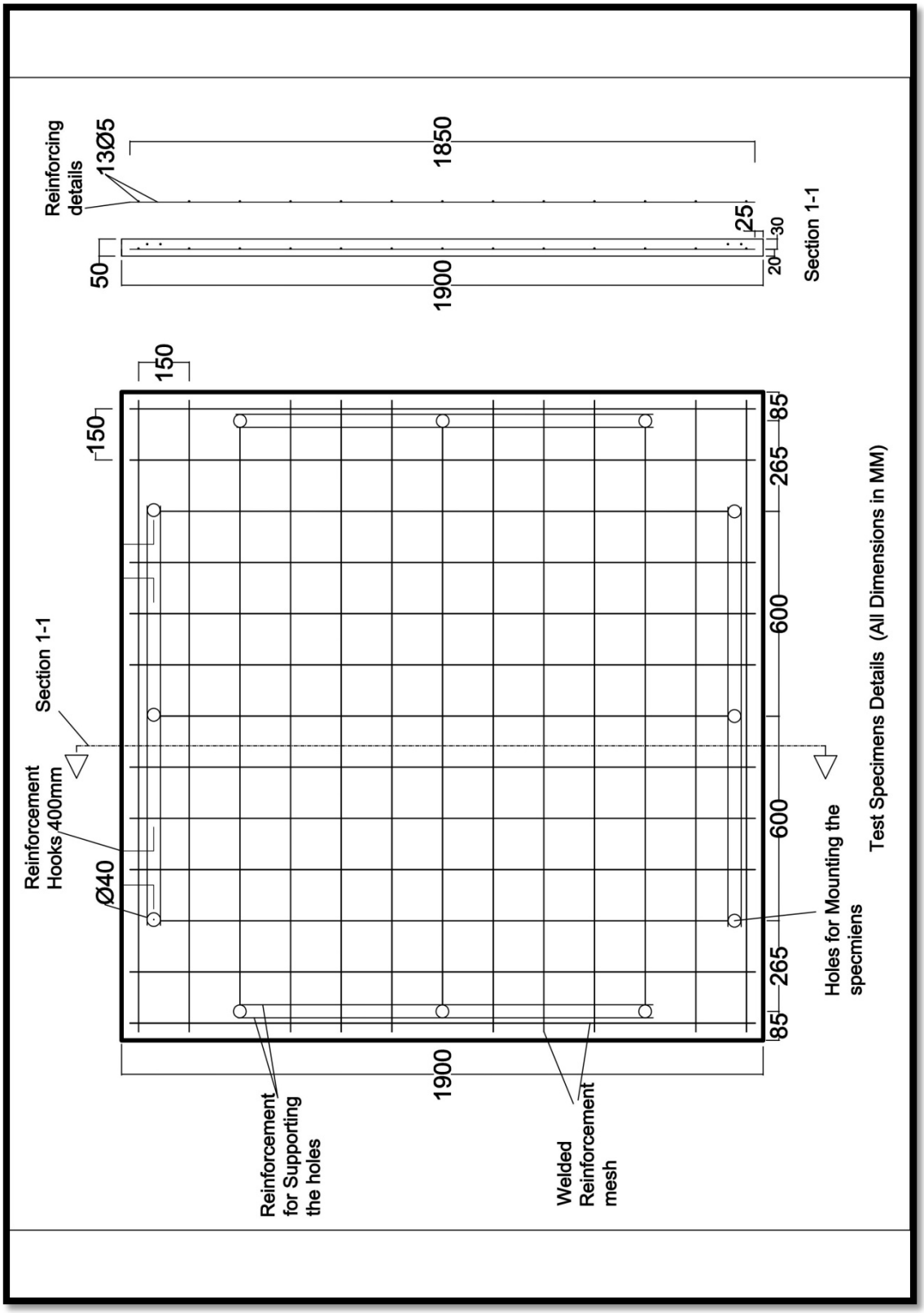

Figure 3.2. Test Specimen Details (All Dimensions in mm)

Figure 3.3. Formwork

3.3. Materials

3.3.1. Concrete

In this study, Portland cement (PC), CEM I 42.5 R was used in all specimens which conformed with TS EN 197-1: 2012. The specific gravity and Blaine fineness of it were 3.06 and 325 m^2/kg relatively.

Class-F fly ash as designated in ASTM C 618 with a specific gravity of 2.61 and Blaine fineness of 290 m^2/kg was used.

20% of the aggregate was taken from crushed limestone coarse aggregate with a maximum size of (D_{max}) 16 mm and 80% was taken from a mixed coarse and fine aggregate. Results of sieve analyses for mixed aggregates and coarse aggregate are shown in Figure 3.4 and 3.5. The coarse aggregate, mixed aggregate, fly ash and cement are shown in Figure 3.6.

To increase the workability of fresh concrete, a polycarboxylic super plasticizer (Master Glenium 21) was used. Expanded perlite aggregate was used in the panel cast with perlite.

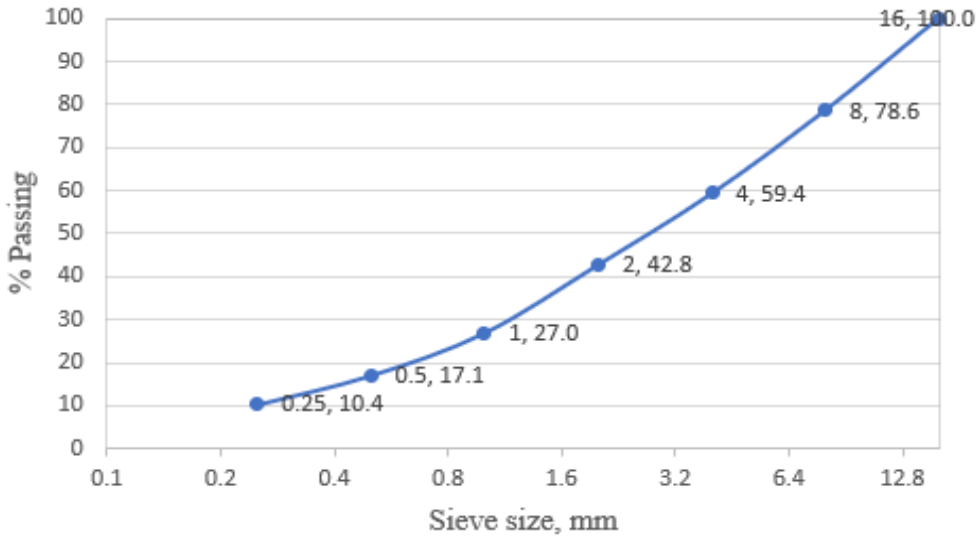

Figure 3.4. Grading Curve for Mixed Aggregate

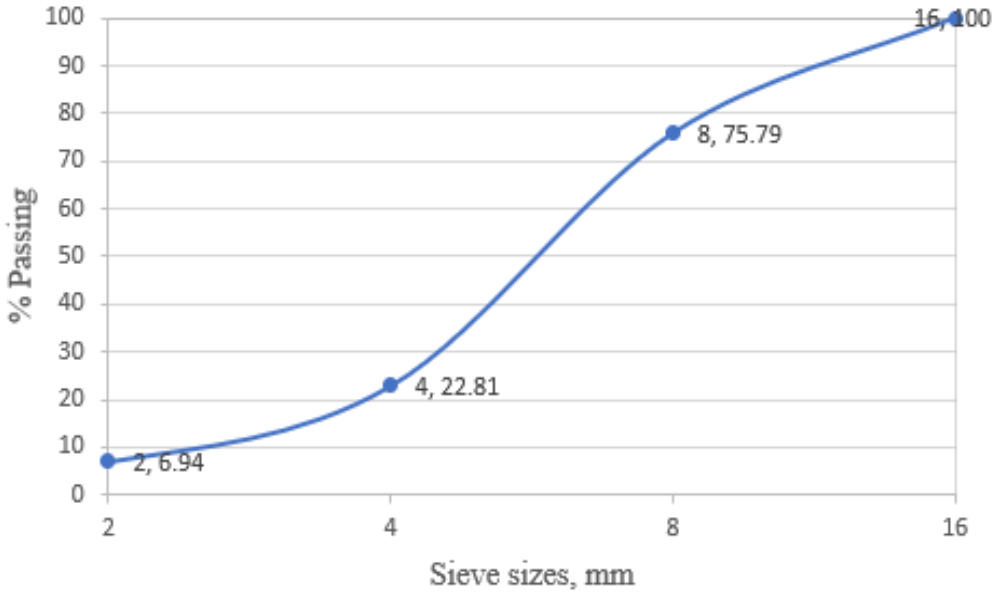

Figure 3.5. Grading Curve for Coarse Aggregate

(a) Coarse aggregate

(b) Mix (coarse & fine) aggregate

(c) Fly Ash

(d) Portland cement

Figure 3.6. Materials for Concrete

3.3.2. Reinforcing Steel and Steel Fibers

5 mm diameter steel bars that were used in some panels were subjected to tension. Stress-strain relationship obtained is given in Figure 3.7. Results showed that the average of yield and ultimate strength were f_y=700 MPa and f_u=735 MPa, respectively.

Different hook-end steel fibers were used in panels, which belonged to Bekaert Dramix brand. Mechanical and geometric properties of three types of steel fibers used are presented in Table 3.1.

Table 3.1. Mechanical and Geometric Properties of Steel Fibers

Steel Fiber Hooked type	Length (mm)	Diameter (mm)	Aspect Ratio	Tensile Strength (Mpa)	Figure
45/35 3D	45	35	0.78	1225	3.8 a
65/60 3D	65	60	0.92	1160	3.8 b
65/60 5D	65	60	0.92	2300	3.8 c

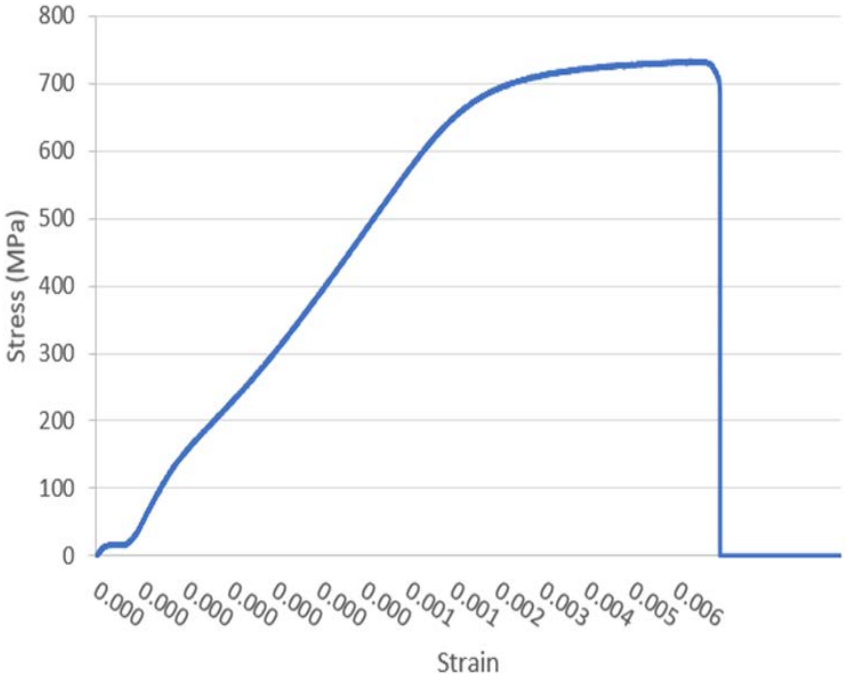

Figure 3.7. Stress-strain Relationship of Reinforcing Bars

(a) 45/35 3D (b) 65/60 3D (c) 65/60 5D

Figure 3.8. Steel Fibers

3.3.3. PVA Fiber

To produce six HyFRC panels, Kuralon K-II RECS 15/8 mm brand Polyvinyl Alcohol fibers were used with steel fibers in the mix design. PVA fibers are shown in Figure 3.9 and the properties are given in Table 3.2.

Figure 3.9. PVA Fiber

Table 3.2. Mechanical Properties of PVA Fibers

Fiber Type	Length (mm)	Diameter (mm)	Specific Gravity	Nominal Strength (Mpa)	Apparent Strength (Mpa)	Strain (%)	Young Modulus (Gpa)
PVA	8	40	1.3	1610	10926	6	42.8

3.4. Construction of Test Specimens

3.4.1. Mixing Procedure, Casting, and Curing

All the mixtures of specimens were produced and mixed at the Construction Materials Laboratory of Izmir Institute of Technology. Two batches were done by using a rotating drum mixer with a 200-liter capacity to cast one panel and get six cylinders (ϕ150 x 300 mm) to find the compressive strength of hardened concrete (Figure 3.10). The concrete was transferred to Structural Mechanics Laboratory by using wheelbarrows to pour in oiled clean wooden formwork (Figure 3.10). Two panels were cast at the same time in two molds. Poured concrete was distributed into formwork using some hand tools, and then compacted by a handheld electrical vibrator (Figure 3.10). A smooth surface was obtained by using a trowel and some hand operation. The panels were cured for one week covering with moistened burlaps and plastic tarps. Later, the curing kept going on for three months in a humid environment at the lab before testing (Figure 3.10). The operation stages of casting concrete is summarized in Table 3.3.

Table 3.3. Operation of Casting Concrete

Stage	Definition
1	Adding the fine (or/and presoaked Perlite in the case of final panel mixture) and coarse aggregates with some water into the mixer, mixing for 3-4 minutes
2	Appending the cement and fly ash into the mixer then supplying the water gradually
3	Mixing very well for 4 minutes and introducing designed amount of superplasticizer
4	If present, adding moistened steel fibers gradually to prevent the balling problem Mixing for 3 minutes
5	If present, adding PVA Fibers gradually to prevent the balling problem Mixing for 4 minutes

(a) Rotating drum mixer

(b) Adding fibers gradually

(c) Transferring by using a wheelbarrow

(d) Pouring &distributing into formwork

(e) Compaction by handheld electric vibrator

(f) Finishing smooth surface

(g) Burlap and plastic for curing

Figure 3.10. Operation of Casting

The mixture of concrete was the same for both the preliminary and main specimens (Table 3.4). However, to cast SFRC panels, different types and content of steel fibers were used as shown in Table 3.5.

Table 3.4. Concrete Mixture Content

Fine aggregate	624 Kg/ m^3
Coarse aggregate	678 Kg/ m^3
Water	240 Kg/ m^3
Cement	274 Kg/ m^3
Fly ash	326 Kg/ m^3
Superplasticizer	1.3 L/ m^3

The weight of steel fibers in 1 m^3 concrete was 58.5 or 97.5 Kg/ m^3 depending on the volume of them in mix design. PVA fiber was 3.25 Kg/ m^3 when present.

Naming convention for mixes were as follows: **JA** (test program identifier) + steel fiber type (1: 45/35 3D, 2: 65/60 3D, 3: 65/60 5D) + steel fiber volumetric ratio (x100) + other materials if present (PVA: presence of PVA fibers, Perlite: presence of perlite, RF: presences of steel reinforcement mesh)

3.4.2. Hardened State Concrete Properties

To determine the compressive strength of concrete that was use in preliminary specimens, 6 cubical (150*150*150 mm) samples were taken from batches. The samples were cast and cured according to Turkish Standards. The average of compressive test results after converting to equivalent cylinder strength was 43 MPa in 28 days.

For each main specimen, six cylinders (300 mm in length and 150 mm in diameter) were cast, cured and tested according to ASTM C39 Standards. The six samples were taken in groups during mixing. Three of them were taken before addition of any fibers and other three after addition of steel and/or PVA fibers. All compression tests were done about after 90 days of casting during the shock tube testing of panels to obtain the concrete strength at the time of testing. Compression tests were done by using a digital compression machine at Construction Materials Laboratory (Figure 3.11).

The compression test results of samples without any fibers were varied between 32 and 46 MPa under a loading rate of 0.6 N/mm^2/s. However, the samples which contained fibers resulted between 39 and 52 MPa. The averages of results are given in Figure 3.12.

Table 3.5. Plain, SFRC and HyFRC Mixture Proportions

Preliminary Specimens					
Panel Type	Specimen Name	Thickness (mm)	Steel Fiber Type	Steel Fiber Volume content (%)	Longitudinal Reinforcement
RC	A0	100	-	-	ϕ10/100mm mesh
SFRC	A1	75	40/30 3D	0.75	-
SFRC	A2	50	40/30 3D	0.75	-

Main Specimens					
Specimen Name	Fiber Type	Steel Fiber Volume content (%)	PVA Fiber Volume content (%)	Steel Reinforcement	Perlite Content
JA1-075	45/35 3D	0.75	-	-	-
JA1-075+PVA	45/35 3D	0.75	0.25	-	-
JA2-075	65/60 3D	0.75	-	-	-
JA2-075+PVA	65/60 3D	0.75	0.25	-	-
JA3-075	65/60 5D	0.75	-	-	-
JA3-075+PVA	65/60 5D	0.75	0.25	-	-
JA2-125	65/60 3D	1.25	-	-	-
JA2-125+PVA	65/60 3D	1.25	0.25	-	-
JA2-075-RF	65/60 3D	0.75	-	ϕ5/150 mm mesh	-
JA2-075-RF+PVA	65/60 3D	0.75	0.25	ϕ5/150 mm mesh	-
JA-Plain-RF	-	-	-	ϕ5/150 mm mesh	-
JA2-075-Perlite+PVA	65/60 3D	0.75	0.25	-	20% of fine aggrega-te

(a) Cylinders before testing

(b) Cylinders placing in machine

(c) Cylinders after testing

Figure 3.11. (a, b &c) Compression Tests With Using a Digital Machine

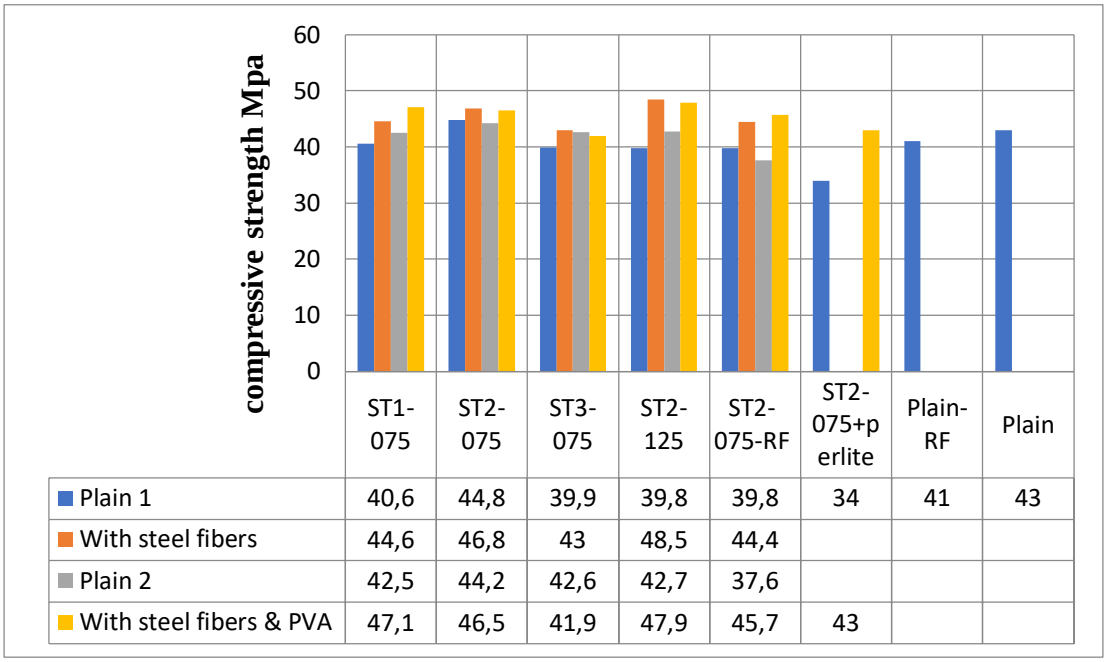

	ST1-075	ST2-075	ST3-075	ST2-125	ST2-075-RF	ST2-075+perlite	Plain-RF	Plain
Plain 1	40,6	44,8	39,9	39,8	39,8	34	41	43
With steel fibers	44,6	46,8	43	48,5	44,4			
Plain 2	42,5	44,2	42,6	42,7	37,6			
With steel fibers & PVA	47,1	46,5	41,9	47,9	45,7	43		

Figure 3.12. The averages of Compression Test Results

3.5. Test Procedure and Instrumentation

The main goal of the experimental program was to compare the behavior with varying types of fiber reinforced concrete panels under blast loading. Two preliminary specimens were tested to decide the thickness of panels for the main specimens through the damage to the panels after the tests. Twelve main panels were tested under blast loads, which were produced by using a shock tube. The shock tube was designed and manufactured in order to simulate blast waves (Figure 3.13). It was composed of four main parts. The driver section, a tube with a variable length between 510 mm and 6300 mm, was manufactured by combining six steel pipes of varying lengths. Two 1500 mm, two 1020 mm, and two 510 mm steel pipes with an outer diameter of 840 mm and an inner diameter of 600 mm were used in this section. For this test program, two 1500 mm and two 510 mm pipes were used, resulting in 4200 mm tube length. The shock wave was generated by filling this tube with high-pressure air coming from the compressor through a high-pressure hose connected to the inlet of driver section. The dead end of the tube was a steel plate. Other end of the tube was closed by an aluminum diaphragm, formed by variable number of aluminum sheets. The highest pressure in the driver section was determined by the rupture strength of the diaphragm. Therefore, different pressures were created by placing different number and thicknesses of aluminum sheets. The rupture strength of the diaphragms were calibrated before testing program commenced and values in Table 3.6 were obtained.

Table 3.6. Rupture Strength of Aluminum Diaphragms

Number of Foils	Thickness (mm)	Rupture Pressure (bar)
1	1	2.5-2.7
2	1	4.7-4.9
2	1.5	6.8-7.0
1	1.5	3.1
3	0.3	0.95-1.15
4	0.3	2.70

The second section was a spool section that contains a double diaphragm firing system intended to control the rupture time of the aluminum diaphragm. However, this system was found difficult and unreliable to operate during the test and therefore disabled for this test program. The third section was an expansion section that connects the driver and spool sections to a test frame. This section is a conical tube that allows high-pressure air, which was suddenly released by the explosion of the aluminum diaphragm, to expand and move forward onto the specimen. The length of this section was 6500 mm, with a 600 mm diameter circular opening at the spool section and a 2300 mm x 2300 mm square testing frame opening at the other end. On the sides of testing frame, 12 pressure relief vents were left to let the air discharge from the tube. These vents will open when the shock wave reaches at the end of frame and create a negative pressure phase in the pressure-time history as the compressed air exits the tube. The details of shock tube are given in Figure 3.14. To prevent the backfire of the shock tube during the explosion, steel supports were manufactured to fix the shock tube to the laboratory rigid wall. Instrumentation was installed on a plywood supported by a steel frame, which was placed at the back of the specimen (Figure 3.15).

Panels were mounted on the testing frame through 12 steel bolts, passing through the holes left in panels during casting. Two or more 100x100x12 mm lubricated steel plates were placed at the bottom and top of samples at support points. Greased spherical washers were put between the plates. These washers prevented vertical displacements, whereas providing free rotation and displacement parallel to the plane of the panel (Figure 3.16). This arrangement provided a moment-free simply supported boundary condition for the specimens.

A high-speed data acquisition system (National Instruments NI PXI-6143 series device) was used to acquire the measurements at rate of 250 Kilo sample/second/channel. LabVIEW software was used to acquire the data. 12 load cells, 5 Resistive Linear Position Transducers (RLPT), 8 piezoelectric accelerometers, 2 piezoelectric dynamic pressure sensors, and a high-speed video camera were used in all tests. Locations of instrumentation are given in Figure 3.17. 5000 kg capacity S type load cells were placed at supporting points in order to measure support reactions. In order to measure the displacements of some points on panels during tests, RLPT's were installed and placed on plywood fixed to a steel frame. Steel rods were used to connect RLPT's to a hinge at the back of the specimens. Attachment of the hinges to specimen surface was provided by steel U-profiles, fixed on the back face of the specimens by epoxy. Accelerometers

with ±5000g range were fixed on the back face of the specimens. Delrin® cylinders were attached to panels by using epoxy, and accelerometers were fixed on these cylinders. Piezoelectric dynamic pressure sensors were embedded into panels through drilled holes, in order to measure the reflected shock wave pressure from the front face of the panel. To measure the pressure in the driver section during the test, a pressure sensor was placed on the dead end steel plate. High-speed camera was used to capture panels' response at 1000 frames per second rate. Moreover, normal videos were also recorded by a video camera. Since the recording time was very limited, the data acquisition system and high speed camera were set to start recording automatically by a trigger mechanism activated by the rupture of the aluminum diaphragm. The details of the instrumentation are given in Figure 3.18.

All the tests were done following a procedure summarized as below:

1-The specimen was mounted at the test frame, support conditions are provided and the instrumentation was installed and calibrated. The high speed camera and studio lights were adjusted.

2-According to the desired reflected pressure and impulse, aluminum sheets were placed at the end of driver tube and strongly closed. Trigger mechanism for the instrumentation was placed.

3-The driver tube was started to be filled by starting the compressor. When the pressure reaches to the rupture strength of the diaphragm, explosion was occurred.

4-The trigger mechanism was activated automatically and the recording was started instantaneously.

5- High-pressure air simulating blast loading hits the sample by passing through the expansion section, completing the test.

In general, two or three shots were performed on each panel specimen. The first was in the elastic range response with 1 mm thick aluminum sheet, while the second and the third were in inelastic range response by using 1.5 mm thick sheet or two 1 mm sheets.

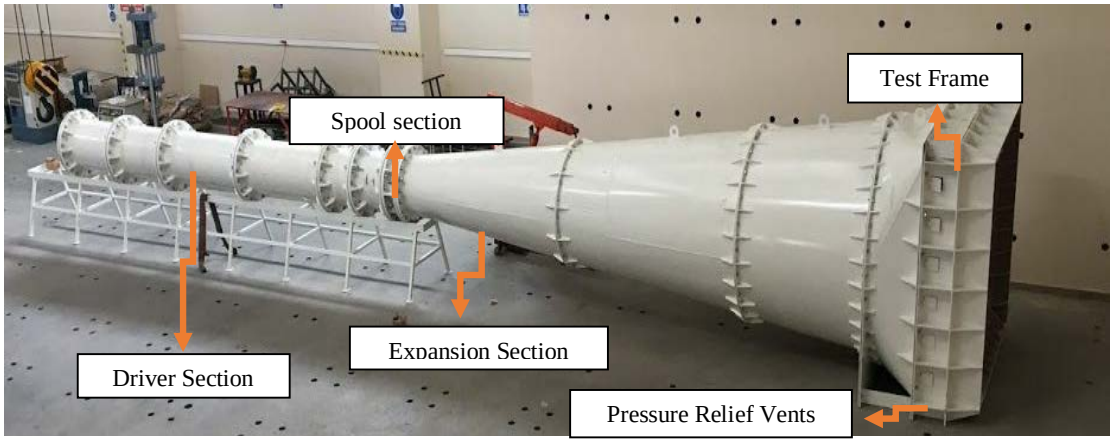

Figure 3.13. Shock Tube

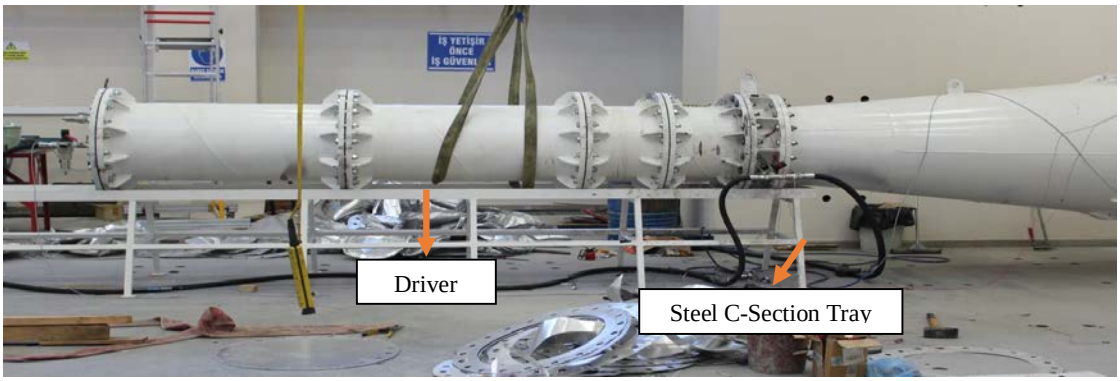

(a) Side view of shock tube

(b) Test frame

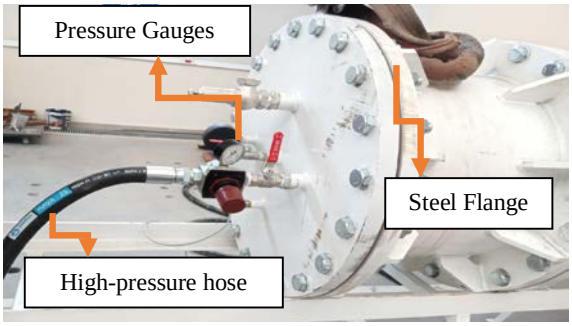

(c) Head of shock tube

(d) Aluminum sheets

(e) Aluminum sheets after testing

Figure 3.14. Details of Shock Tube

(a) Rigid steel frame

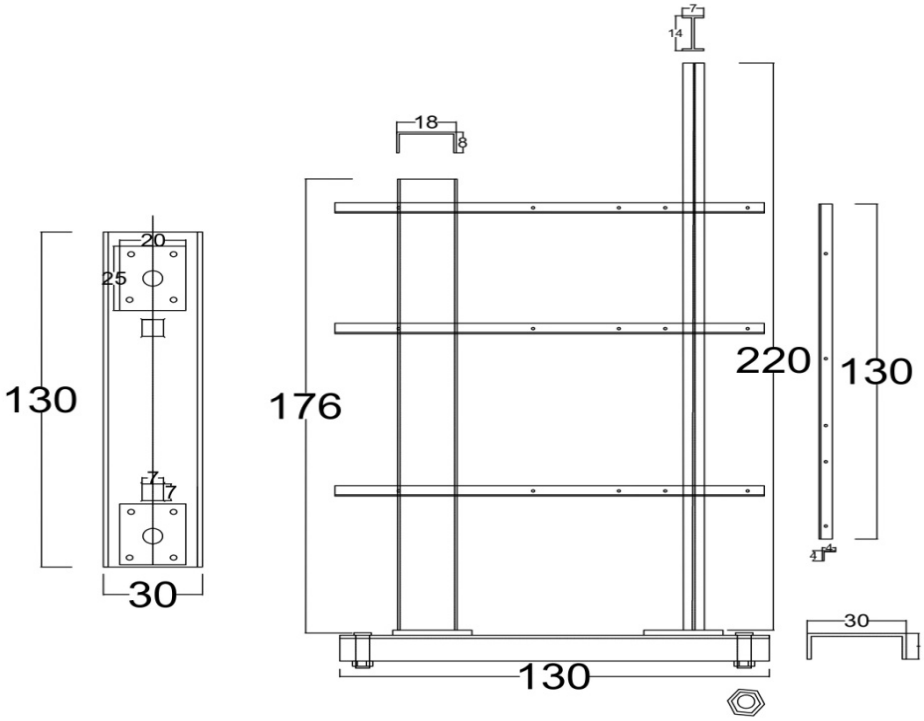

(b) Front view of rigid steel frame

Figure 3.15. Supporting Frame and Instrumentation Frame (All Dimensions in cm)

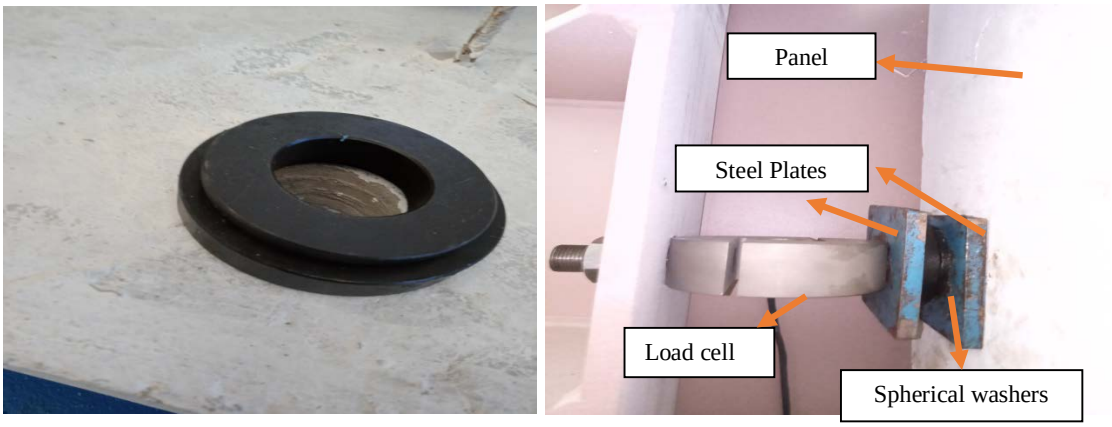

(a) Spherical washers (b) Side view of supporting point

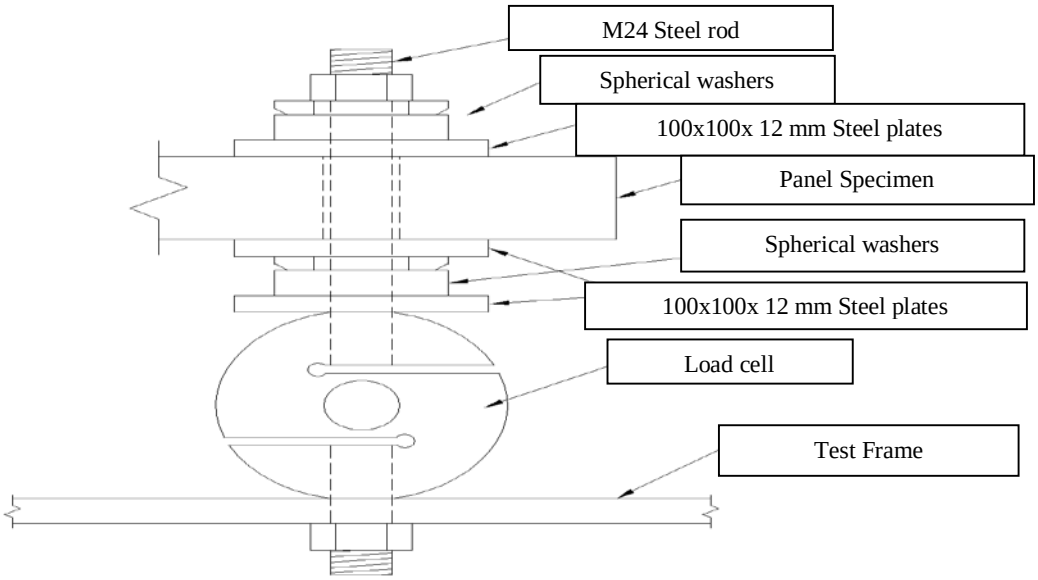

(c) Top view of supporting point

Figure 3.16. Details of Supporting Points

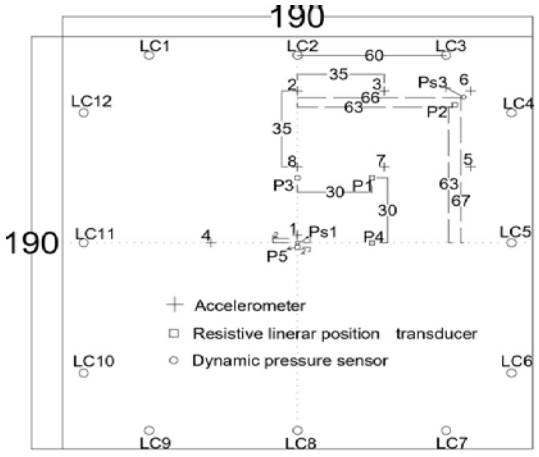

Figure 3.17. RLPT, Accelerometer, Dynamic Pressure Sensor and Load Cell Locations (All Dimensions in cm)

(a) High speed camera

(b) RLPT

(c) load cell

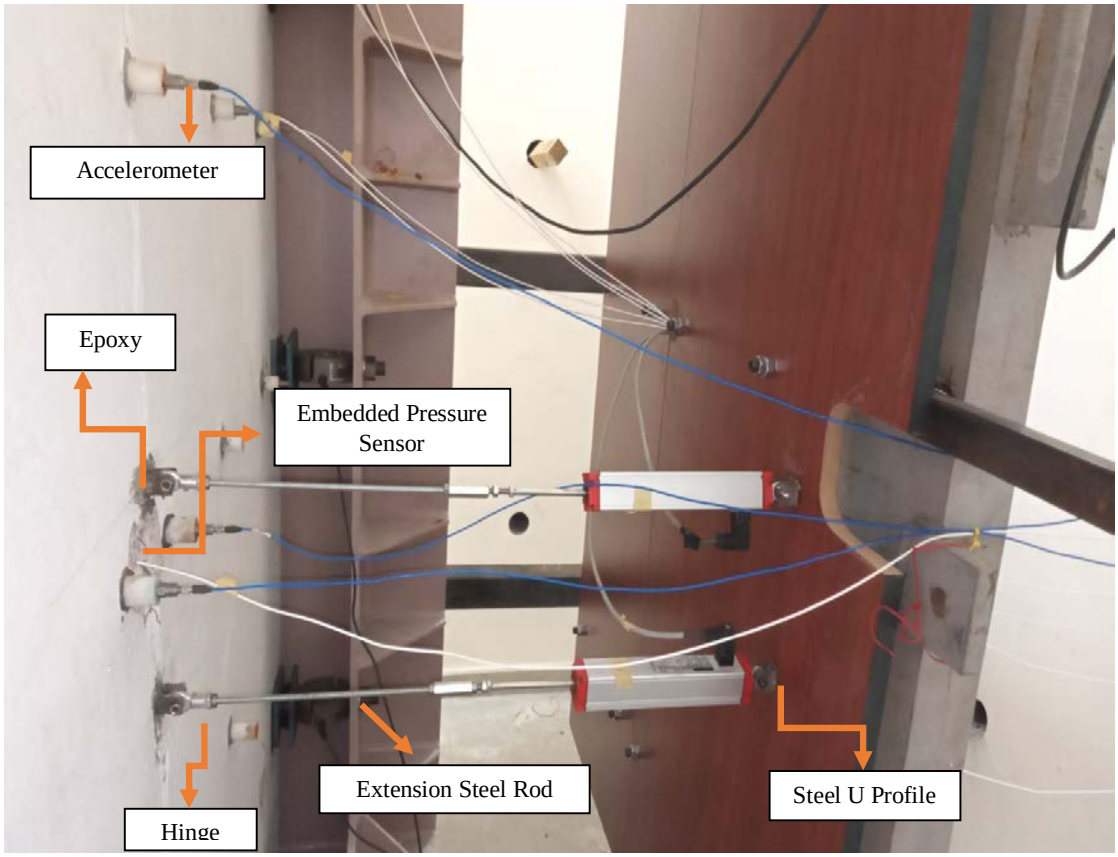

(d) Installing of instrumentations

(e) Compressor

(f) Data Acquisition System

Figure 3.18. Instrumentations

CHAPTER 4

TEST RESULTS AND DISCUSSION

4.1. General

In this chapter, the results obtained from tests are explained and discussed. Shock wave properties, maximum deflections, reflected pressures, reflected impulses, and reactions are presented. The structural behavior of panels under blast loading is compared and discussed with respect to effects of percentage and type of steel fibers, effects of adding PVA fibers and presence of ordinary steel reinforcement.

8.2. Preliminary Tests

As mentioned before, the preliminary specimens were consisted of a rigid panel A0, and two thin panels, A1 (75 mm) and A2 (50 mm). Several tests were performed on A0 to test the shock tube, find rupture pressures of aluminum sheets and calibrate some instrumentation. A2 was subjected to a simulated explosion with a driver pressure above 7 bar. This panel immediately failed and fragmented in a brittle manner when the high pressure shock wave hit the panel (Figure 4.1). As a result, some damage in devices was seen and data were not recorded. After this experience, driver pressure was limited to around 4 bars for all other experiments. A1 was subjected to a simulated explosion with 3 bars of driver pressure. This test was done using the double diaphragm firing mechanism, but the process failed due to two reasons: uncertainty about the exact rupture strength of aluminum sheets and the low data recording time due to uncertainty about the exact time of rupture. Therefore, double diaphragm firing system was disabled for main tests. Instead, a trigger mechanism was installed to start the data acquisition system and high-speed camera.

After preliminary tests, it was decided to test the main specimens first at a driver pressure of around 4 bars. Then, one or two more tests were executed depending on the level of damage that occurred in the specimen. Heavily damaged specimens were subjected to another shock wave blast loading with a lower driver pressure. However, the

specimens that were not damaged much were subjected to another shock wave blast loading with a driver pressure around 4 bars. In this process, the reserve capacities of the panels were determined after the first shock.

Figure 4.1. A2 Specimen After Test

8.3. Main Tests

A characteristic blast waveform is given in Figure 4.2, which represents pressure generating from a free-air detonation. When such a blast wave interacts with a solid surface, it reflects while applying a pressure on the hit surface. This pressure is called reflected pressure and it is the pressure that is significant from the structural point of view. The form of reflected pressure also resembles to free-air pressure wave. In this test program, reflected pressure was measured on the specimens' surface by two piezoelectric dynamic pressure sensors. As an example, the average of the reflected pressure on the surface of the panel of two points, one in the middle and other at the corner of the panel, is illustrated in Figure 4.3.

As it is seen, the shock tube was able to generate shock waves with similar properties as those produced by an actual detonation of high explosives. As seen from Figure 4.3, some secondary shock waves were created due to the interaction of the shock wave with the shock tube walls. Varying shock wave properties were observed in all tests. Different

blast pressure and shredding shape were noted for the same thickness of aluminum sheets due to the following reasons: inability to tighten the bolts of tubes when the diaphragms are installed with the same power every time, variability in the strengths of sheets, pre-existing bending of sheets, and some weaknesses created when opening the holes for the bolts to pass into the sheets. Even if the aluminum sheets ruptured at the same pressure, the pressure-time relationship and blast loads were found different from each other for the same reasons. To ease the comparison, evaluation, and numerical modeling studies, the reflected pressure-time relationship was idealized as shown in Figure 4.4. In this idealization, negative phase of the pressure wave was neglected since it was much smaller in magnitude compared to positive phase and less significant from the structural point of view. The pressure wave was assumed to suddenly raise from zero to the maximum pressure value and then decrease to zero linearly against time. The maximum pressure was assumed to be equal to the maximum average pressure measured in the test. The equivalent positive phase duration t_{rf} was calculated as in Equation 4.1 to give the same impulse with the one measured in the test. In this equation, i^+ is the positive impulse measured in the test, as the area under pressure-time diagram for the positive phase.

$$t_{rf} = \frac{2i^+}{P_{max}} \tag{4.1}$$

According to this idealization, parameters of the pressure wave of all experiments are given in Table 4.1. The number following the specimen name indicates the test number carried on the same specimen. t_a represents the time it took for the shock wave to reach the specimen after the diaphragm ruptured.

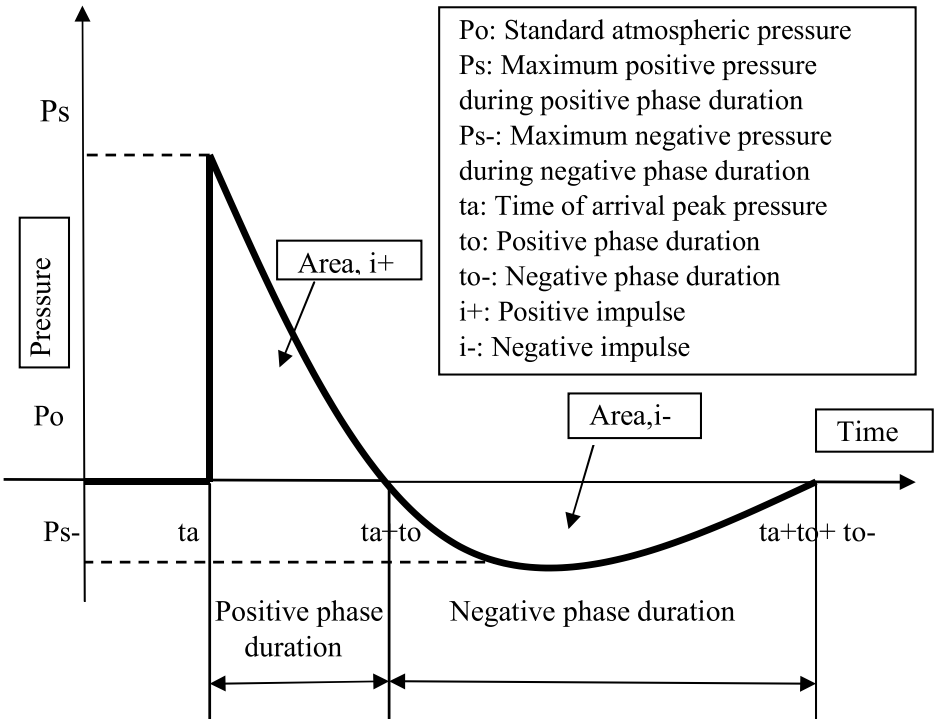

Figure 4.2. Characteristic Blast Pressure Waveform
(Source: Baker, W. E., 1973)

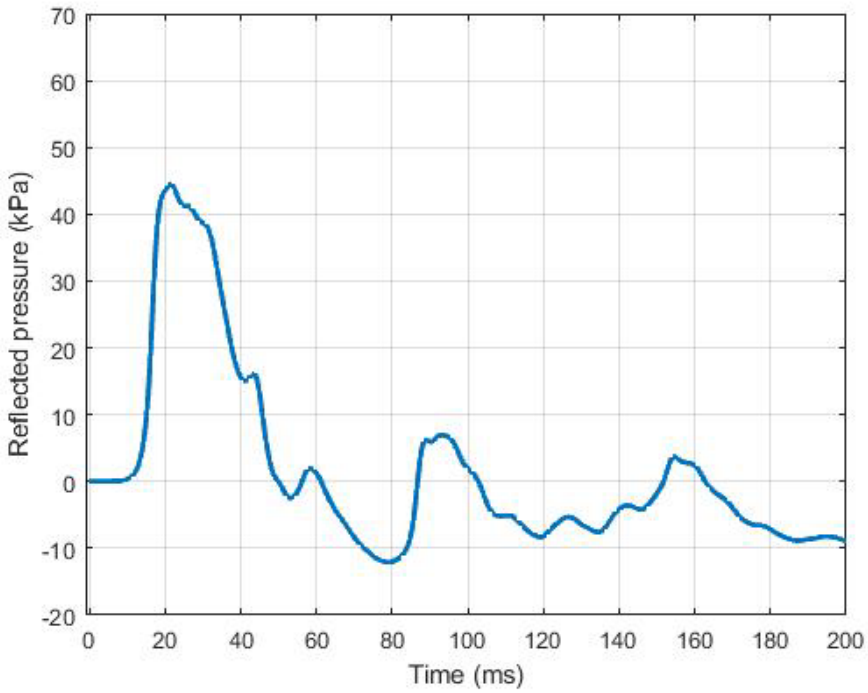

Figure 4.3. Typical Reflected Pressure-time History Generated by the Shock Tube (JA1-0.75)

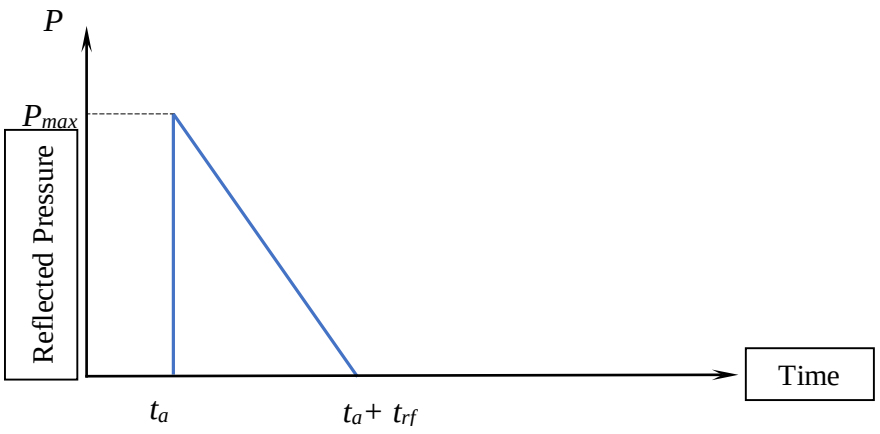

Figure 4.4. Idealized Pressure-time History

As mentioned in the previous section, displacements, support reactions, and accelerations were measured during the test. The maximum values of midpoint displacements, total positive and negative support reactions and midpoint accelerations are given in Table 4.2. As known, the maximum deflection of the panel occurred at the midpoint, so the RLPT was installed there. However, in some tests, the deflection exceeded the capacity of the device and the maximum displacement was not recorded. In these cases, to find the deflection history, the acceleration data taken at the same point was integrated twice. However, displacements obtained from the integration method were not as reliable as the RLPT because of the high noise in the accelerometer recording. In addition, after the peak point of acceleration, unreasonable results were found for displacements. Therefore, displacement values calculated from this method should be used with caution. If the whole shock tube was a closed container and there was enough time for the situation come to a rest, the pressure on the specimen could be calculated according to Boyle's Law as given in Equation 4.2, where V1 is the volume of the driver section, V2 is the volume of the expansion section, P1 the driver pressure before explosion and P2 the Static pressure in the whole shock tube after explosion. These calculated pressures and sample values are given in Table 4.3. As seen in this table, measured maximum dynamic reflected pressures are consistently about 25% higher than the calculated static pressures. Although no detailed calculations were carried out for the dynamic shock tube problem, this consistency in the relation between the calculated and measured pressures can be seen as an evidence on the consistency and repeatability of the shock tube tests.

Boyle's Law $$P2 = \frac{P1xV1}{V1+V2} \quad (4.2)$$

Table 4.1. Blast Pressure Parameters

Specimen	Peak Pressure, Pmax (kPa)	Pressure Arrival Time, ta (ms)	Positive Phase Impulse, i+ (kPa-ms)	Equivalent Positive Phase Duration, trf (ms)	Diaphragm Burst Pressure (bar)
JA1-075	51	16	965	38	3.8
JA1-075+PVA	51	17	710	28	3.8
JA2-075-1	77	17	1100	29	3.7
JA2-075-2	63	16	965	31	3.3
JA2-075+PVA-1	48	17	592	24	3.8
JA2-075+PVA-2	34	16	481	28	2.5
JA3-075-1	41	16	652	32	3.0
JA3-075-2	46	17	523	23	2.0
JA3-075+PVA-1	43	16	633	29	3.1
JA3-075+PVA-2	32	17	438	28	2.4
JA2-125-1	40	15	531	27	3.0
JA2-125-2	47	16	660	28	3.7
JA2-125+PVA-1	52	17	722	28	3.8
JA2-125+PVA-2	36	16	497	28	2.6
JA2-075-RF-1	50	16	840	34	3.9
JA2-075-RF-2	34	18	565	33	2.5
JA2-075-RF-3	59	17	1141	38	4.6
JA2-075-RF+PVA-1	46	18	759	33	3.1
JA2-075-RF+PVA-2	45	15	824	37	3.1
JA2-075-RF+PVA-3	65	16	892	27	4.3
JA2-075-Perlite+PVA-1	50	17	760	30	3.7
JA2-075-Perlite+PVA-2	34	17	450	26	2.5
JA2-075-Perlite+PVA-3	64	16	1447	45	4.8
JA-Plain-RF-1	44	17	937	42	3.5
JA-Plain-RF-2	34	17	533	31	2.6
JA-Plain-RF-3	224	16	5257	47	4.3

Table 4.2. Maximum Response Value

Specimen	Max. Midpoint Displ. (Potentiom-eter) (mm)	Max. Total Positive Reaction (kN)	Max. Total Negative Reaction (kN)	Max. Midpoint Displ. (Accelerometer) (mm)	Max. Mid point Acceler ation (m/s2)
JA1-075	> 87*	40	6	130	614
JA1-075+PVA	> 79*	21	29	117	534
JA2-075-1	62	25	7	55	538
JA2-075-2	> 49*	20	7	96	562
JA2-075+PVA-1	> 82*	14	26	58	595
JA2-075+PVA-2	> 61*	10	9	58	425
JA3-075-1	36	13**	13**	34	491
JA3-075-2	46	7	6	39	349
JA3-075+PVA-1	43	20	15	37	499
JA3-075+PVA-2	> 55*	16	6	50	377
JA2-125-1	18	12	16	19	415
JA2-125-2	62	12	18	60	556
JA2-125+PVA-1	53	10	16	46	508
JA2-125+PVA-2	> 43*	10	12	60	428
JA2-075-RF-1	24	16	16	23	443
JA2-075-RF-2	28	12	9	26	337
JA2-075-RF-3	60	22	51	61	704
JA2-075-RF+PVA-1	-***	14	18	11	380
JA2-075-RF+PVA-2	15	13	13	19	390
JA2-075-RF+PVA-3	-***	18	15	37	500
JA2-075-Perlite+PVA-1	66	16	15	-****	497
JA2-075-Perlite+PVA-2	> 47*	12	16	49	388
JA2-075-Perlite+PVA-3	> 39*	21	25	201	682
JA-Plain-RF-1	> 80*	25	19	45	471
JA-Plain-RF-2	> 63*	24	10	46	397
JA-Plain-RF-3	-***	28	17	122	783

* Maximum value recorded before reaching maximum measurement range
**Cable for LC10 was broken during the test. LC6 data was used to find total reaction
*** Recording is not available due to instrument failure
**** Recording is not reasonable after a certain time

Table 4.3. Maximum Reflected Static Pressure

V1 Volume of the driver section (m3)	V2 Volume of the expansion section (m3)	P1 Driver pressure before explosion (kPa)	P2 Static pressure in the whole shock tube after explosion (kPa)	P2 Measured maximum dynamic reflected pressure (kPa)	Diffe-rence between static and dynamic pressure (%)
4.54	37.83	380	41	51	25
4.54	37.83	250	27	34	26
4.54	37.83	240	26	32	24
4.54	37.83	380	41	52	27
4.54	37.83	480	52	64	24

4.4. Discussion of Results

Results obtained from tests are discussed through comparison of the specimens that have identical steel fiber content.

4.4.1. JA1-075 and JA1-075+PVA Tests

Both panels were subjected to one blast. The peak reflected pressure was very close for both. However, the impulse imposed on JA1-075+PVA was 25% less than the one for JA1-075. For both specimens, the maximum displacements at the midpoint exceeded the capacity of the RLPT device. The maximum displacement in JA1-075 and JA1-075 + PVA, which was calculated by the integration method, was 117 mm and 130 mm, respectively. The extent of damage and the crack patterns after testing are presented in Figures 4.4.1 to 4.4.4. Very wide cracks close to diagonals and many other narrower cracks were developed after testing in both specimens. The number of cracks and the spacing between cracks were similar. The deflection in both panels was very high. For these samples, there was no significant difference between the behavior of the hybrid fiber panel and the only steel fiber panel.

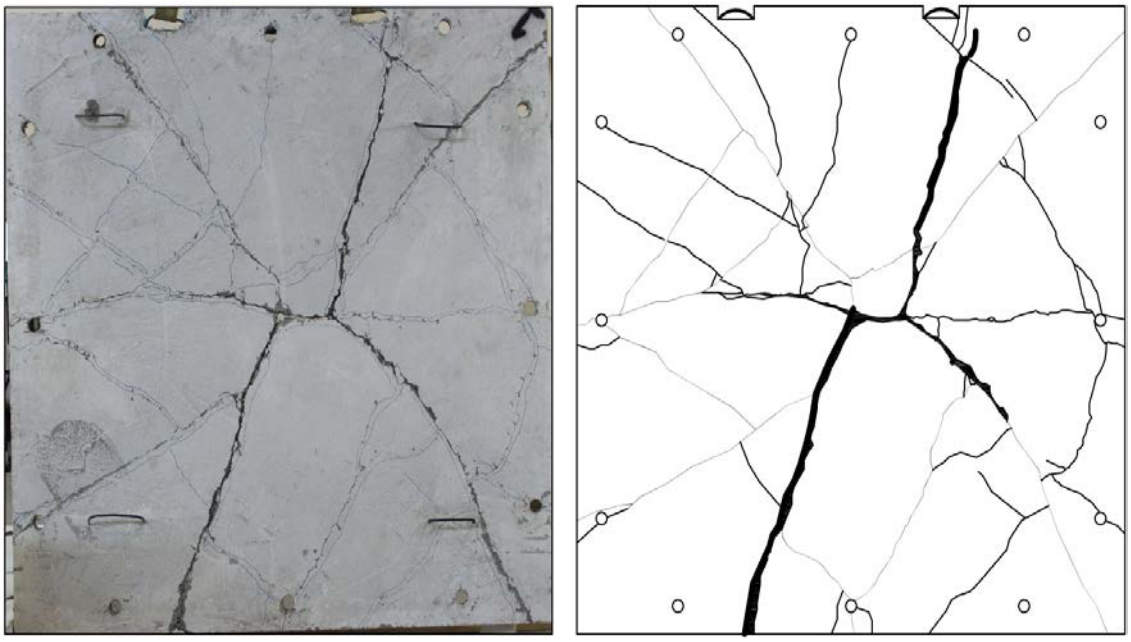

Figure 4.4.1. Front Face Crack Patterns After Testing for Panel JA1-075

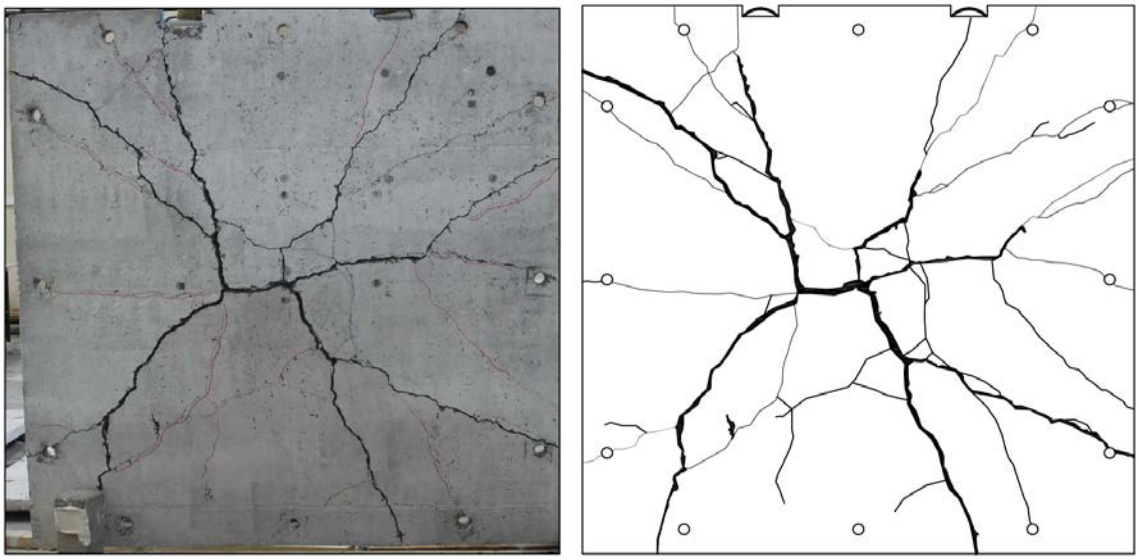

Figure 4.4.2. Rear Face Crack Patterns After Testing for Panel JA1-075

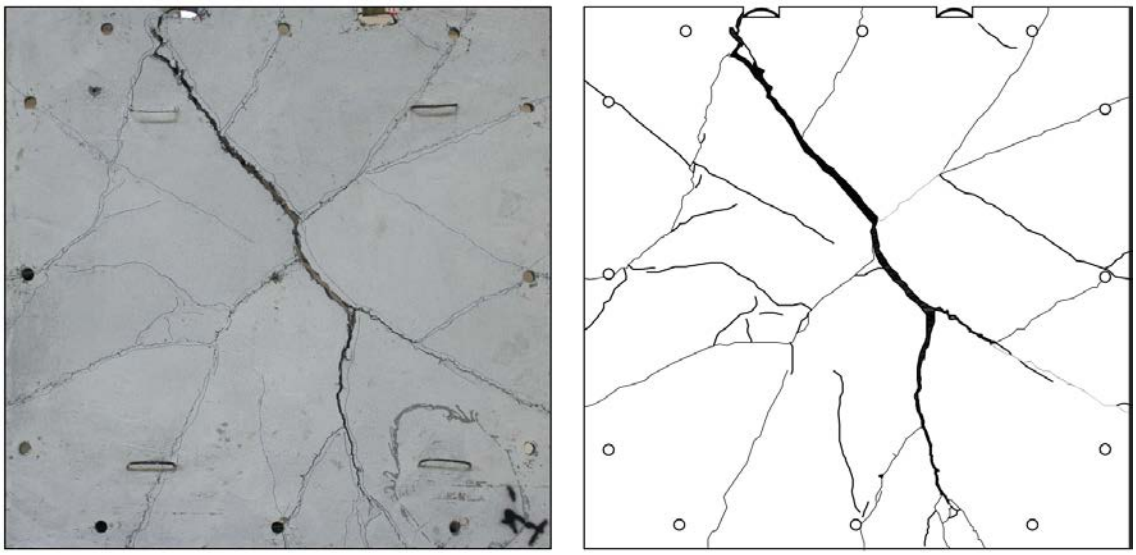

Figure 4.4.3. Front Face Crack Patterns After Testing for Panel JA1-075+PVA

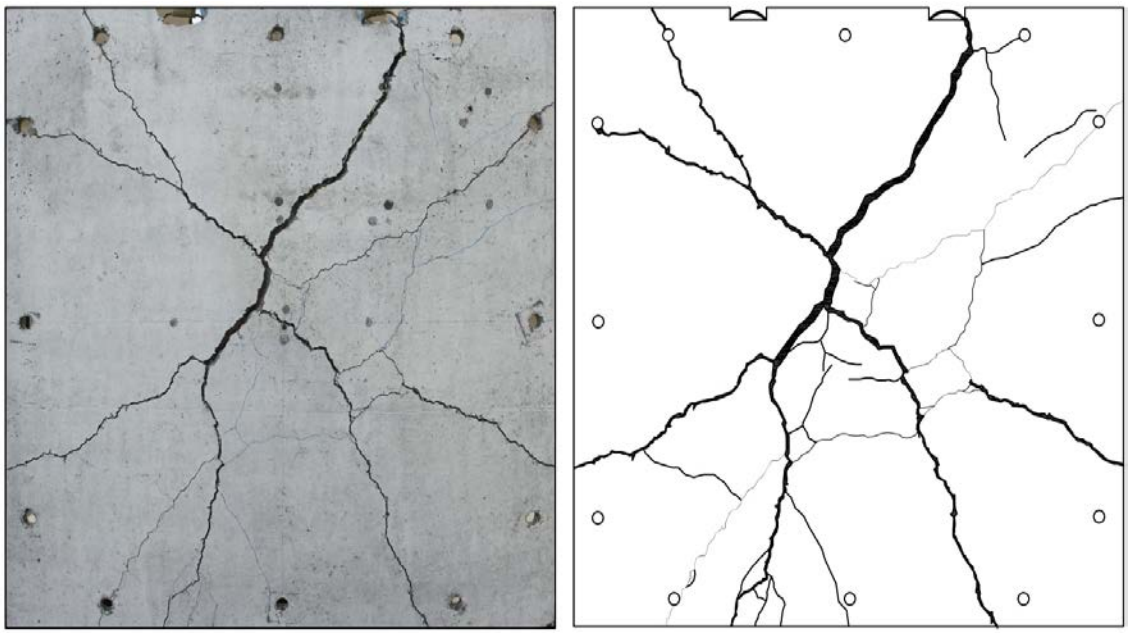

Figure 4.4.4. Rear Face Crack Patterns After Testing for Panel JA1-075+PVA

4.4.2. JA2-075, JA2-075+PVA and JA2-075-Perlite+PVA Tests

JA2-075 and JA2-075+PVA were tested twice and JA2-075-Perlite+PVA was tested three times. The maximum reflected pressure and reflected impulse recorded for

JA2-075 for both tests were higher than JA2-075+PVA and JA2-075-Perlite+PVA. The cracks that were developed on the surfaces of the specimens are shown in Figures 4.4.5 to 4.4.10.

Large and extensive diagonal through-thickness cracks were seen on the front and back face of the JA2-075-Perlite+PVA specimen after completing three tests. Heavy damage was observed at the middle region of the specimen. The panel fragmented almost into three pieces. More hair-line cracks were formed in the JA2-075+PVA when compared to other specimens. Although JA2-075+PVA and JA2-075-Perlite+PVA were subjected to approximately 46% and 31% lower impulses compared to the JA2-075 for the first blast, respectively, the reduction in maximum displacements were at a lower rate. The displacement, which was recorded at the mid-point of the JA2-075+PVA specimen by RLPT, may not be correct because the capacity of the device was exceeded. However, the value that was calculated by the integration method is more logical. Although the displacements were found similar in the three specimens, the width of the cracks in JA2-075+PVA was smaller and narrower.

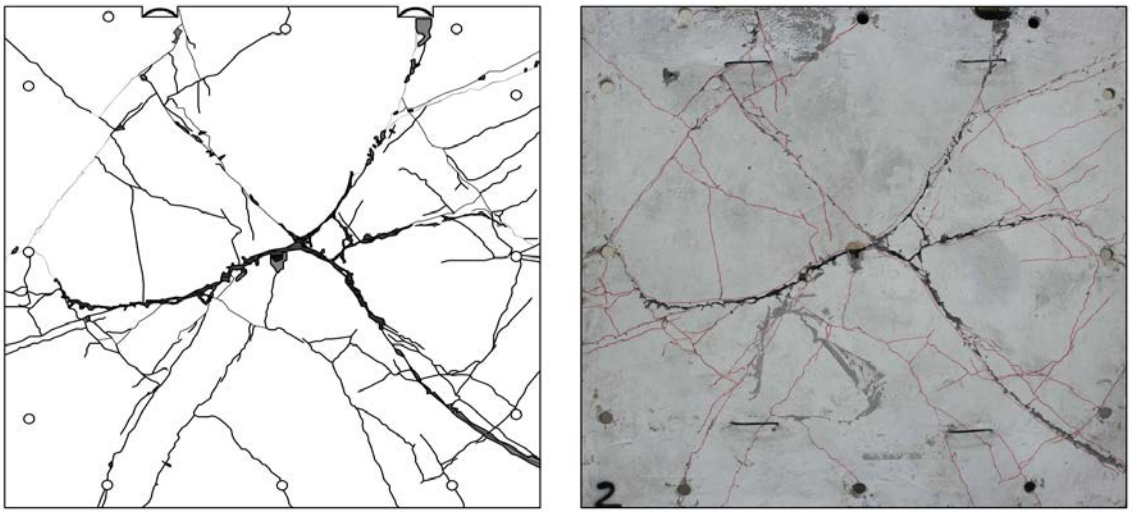

Figure 4.4.5. Front Face Crack Patterns After Testing for Panel JA2-075

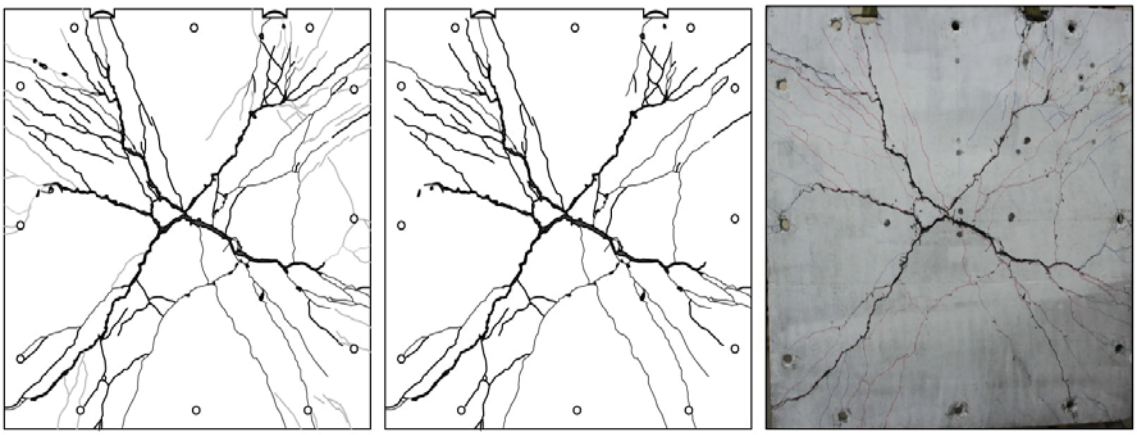

Figure 4.4.6. Rear Face Crack Patterns After Testing for Panel JA2-075

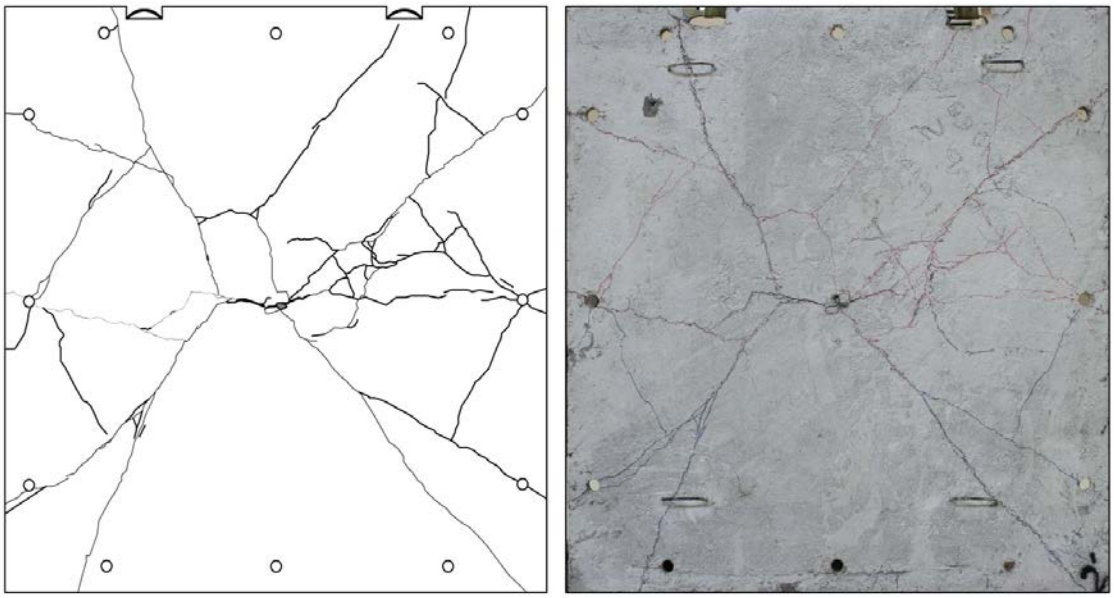

Figure 4.4.7. Front Face Crack Patterns After Testing for Panel JA2-075+PVA

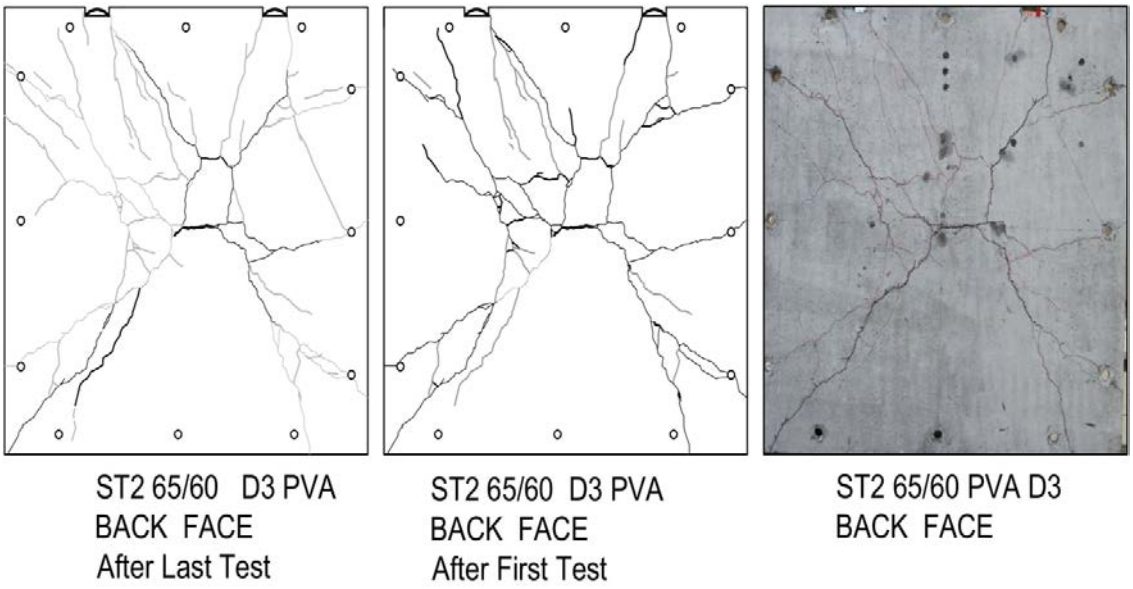

Figure 4.4.8. Rear Face Crack Patterns After Testing for Panel JA2-075+PVA

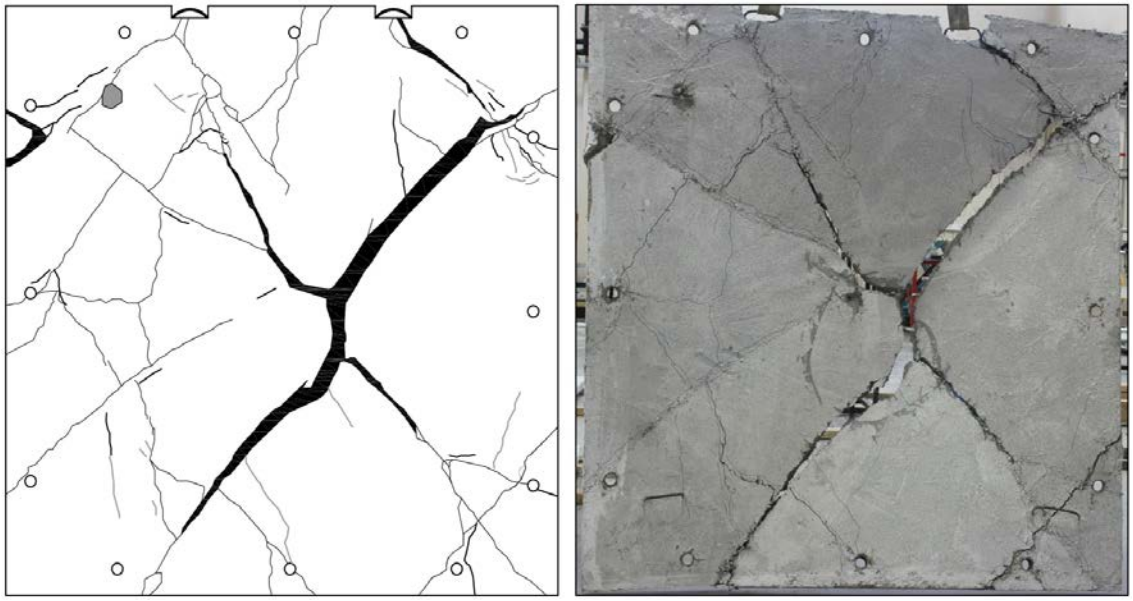

Figure 4.4.9. Front Face Crack Patterns After Testing for Panel JA2-075-Perlite+PVA

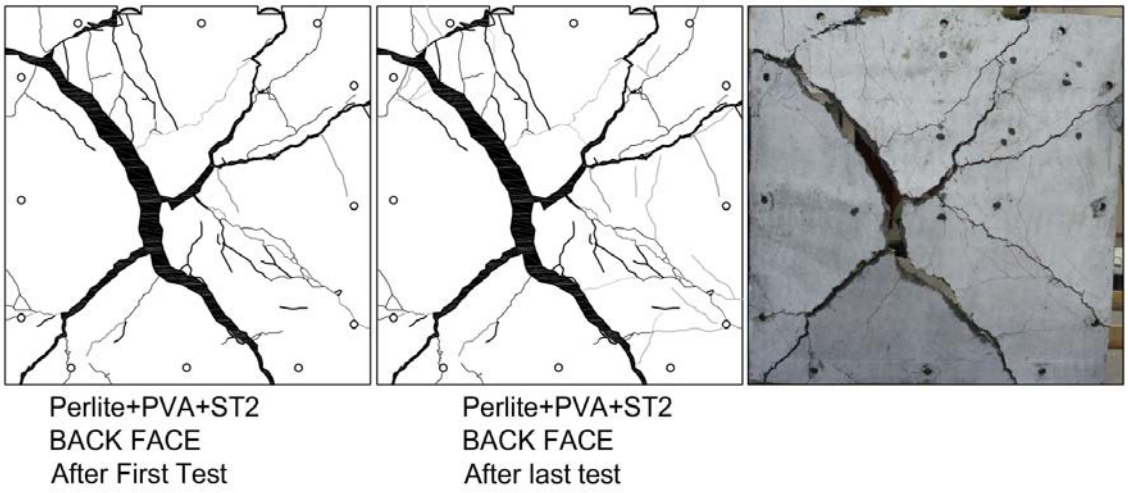

Figure 4.4.10. Rear Face Crack Patterns After Testing for Panel JA2-075-Perlite+PVA

4.4.3. JA3-075 and JA3-075+PVA Tests

JA3-075 and JA3-075+PVA specimens were both subjected to two simulated explosions. In the first test, the impulse was very close in both specimens, but in the second test, the recorded impulse for JA3-075+PVA was 16% lower compared to the other. More deformation was noted at the midpoint of the JA3-075+PVA than JA3-075. The crack patterns after testing are presented in Figures 4.4.11 to 4.4.14. As shown in JA3-075+PVA, cracks were narrower and less in number compared to JA3-075.

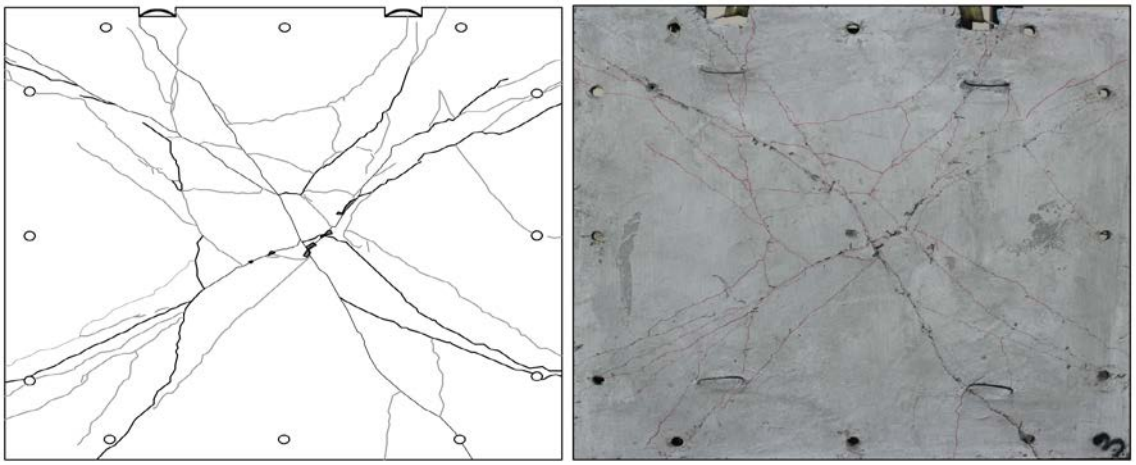

Figure 4.4.11. Front Face Crack Patterns After Testing for Panel JA3-075

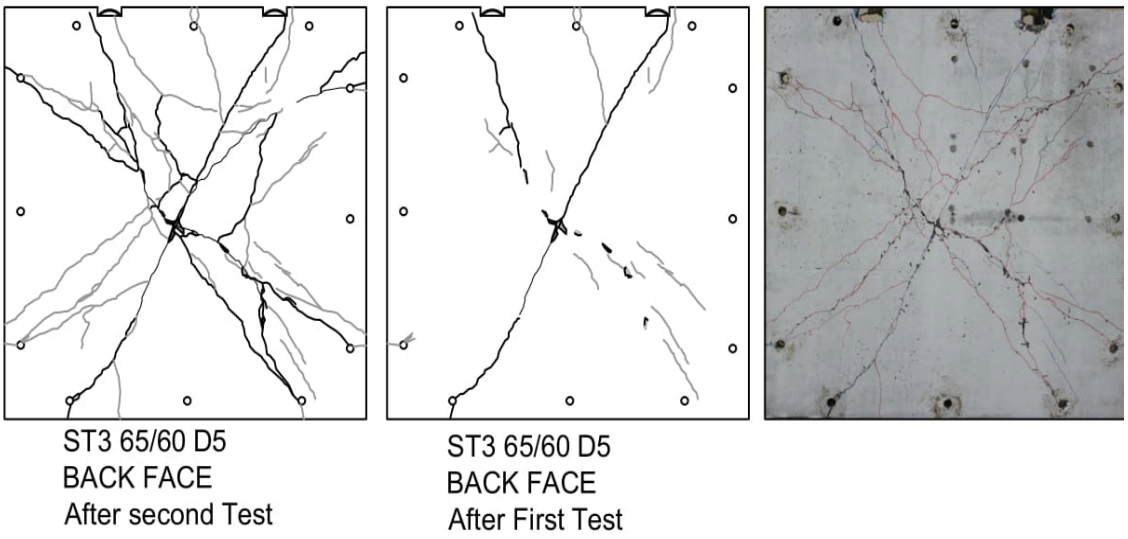

Figure 4.4.12. Rear Face Crack Patterns After Testing for Panel JA3-075

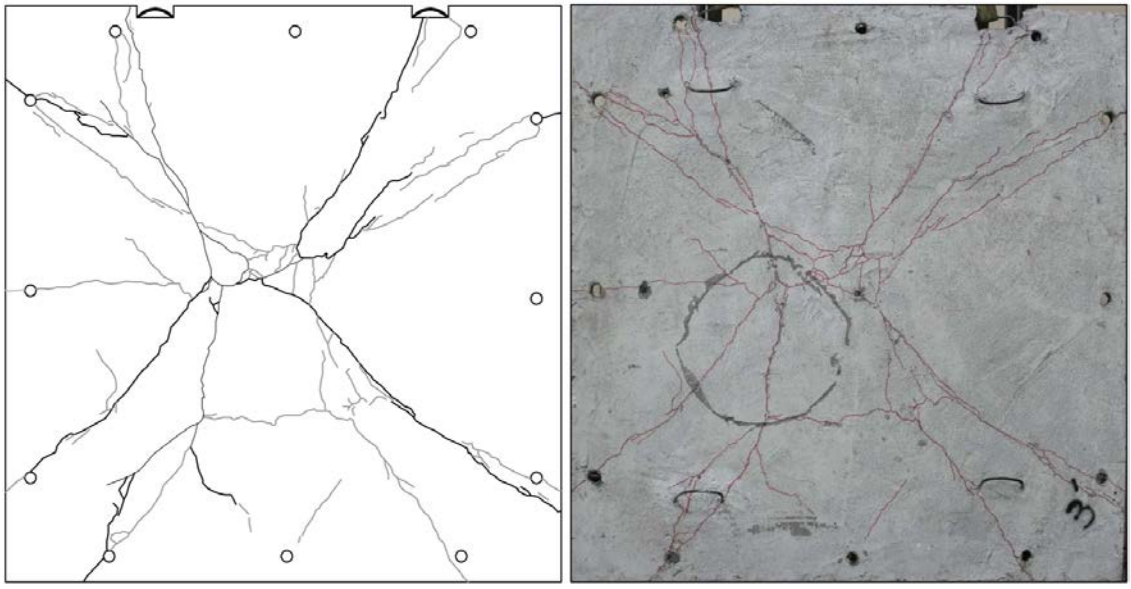

Figure 4.4.13. Front Face Crack Patterns After Testing for Panel JA3-075+PVA

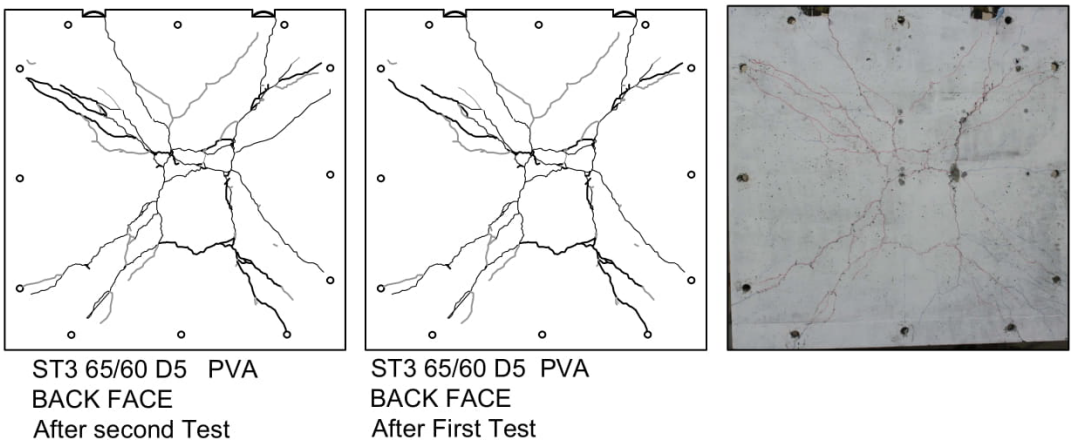

Figure 4.4.14. Rear Face Crack Patterns After Testing for Panel JA3-075+PVA

4.4.4. JA2-125 and JA2-125 +PVA Tests

JA2-125 and JA2-125+PVA specimens were both tested twice under simulated blast loads. As seen in Table 4.1, in the first test of JA2-125, measured impulse was 26% lower than JA2-125+PVA. On the other hand, in the second test, impulse on JA2-125 was 25% higher. The peak displacement at midpoint in JA2-125 panel was less than half the displacement in JA2-125+PVA for the first tests. However, in second tests, measured displacements were close for both specimens. Crack profiles after testing are illustrated in Figures 4.4.15 to 4.4.18. As can be seen from the figures, in both specimens, crack profiles were similar. However, for JA2-125+PVA, cracks were narrower and less in number compared to JA2-125.

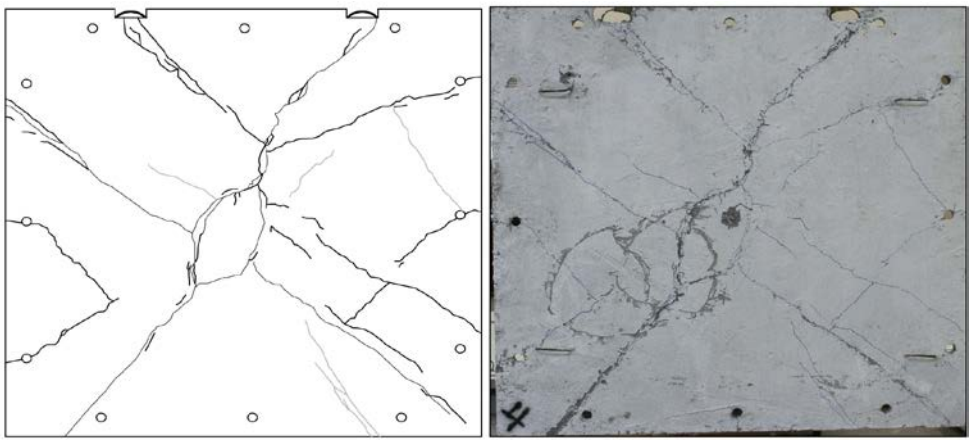

Figure 4.4.15. Front Face Crack Patterns After Testing for Panel JA2-125

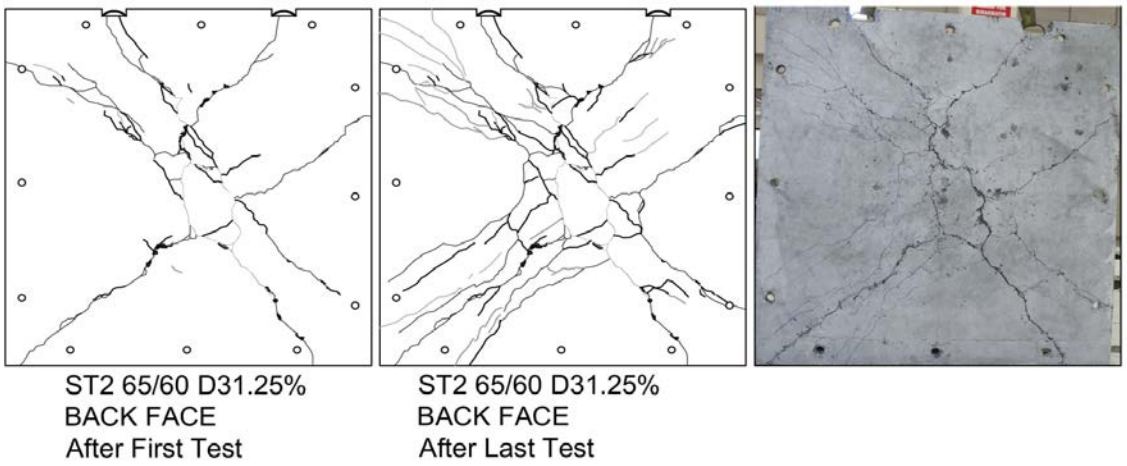

Figure 4.4.16. Rear Face Crack Patterns After Testing for Panel JA2-125

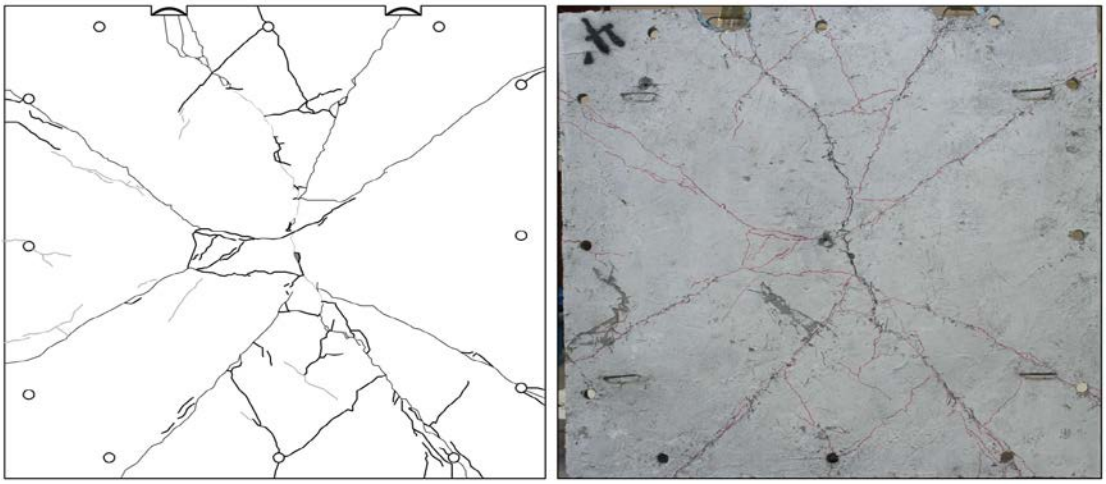

Figure 4.4.17. Front Face Crack Patterns After Testing for Panel JA2-125+PVA

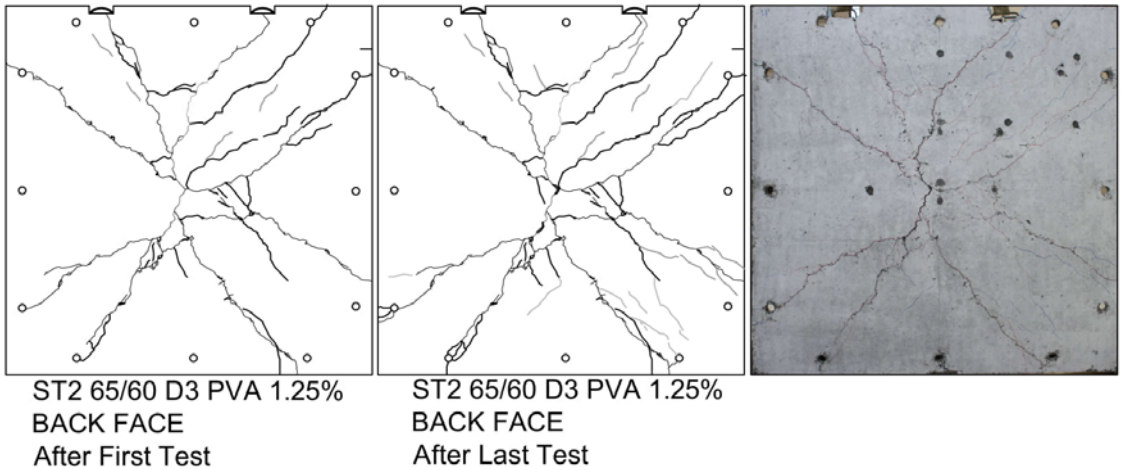

Figure 4.4.18. Rear Face Crack Patterns After Testing for Panel JA2-125+PVA

4.4.5. JA2-075-RF, JA2-075-RF+PVA and JA-Plain-RF Tests

JA2-075-RF and JA2-075-RF+PVA samples were tested both three times. Reflected impulses were close for the first tests for both specimens. However, in the second test, impulse for JA2-075-RF+PVA was 31% higher compared to the second test of JA2-075-RF, due to the premature explosion of the aluminum diaphragm in JA2-075-RF-1. Because of the low damage in the first two tests, a higher driver tube pressure was selected in the third test and higher impulses were obtained. The peak displacements at midpoints for both specimens were less than other panels since they contained additional steel reinforcement. When panels were compared to each other, the peak displacement at midpoint of JA2-075-RF+PVA was less than JA2-075-RF for all tests. The crack patterns after testing are presented in Figures 4.4.19 to 4.4.22. As can be seen from the figures, both specimens suffered limited damage compared to other specimens, despite being tested three times and exposed to higher impulses. In both samples, the number of cracks were more, but the crack widths were small. In this group, cracks were narrower in the hybrid fiber JA2-075-RF+PVA compared to the other.

Impulse for JA-Plain-RF was higher for the first test and lower for the second test than other steel reinforced specimens. However, impulse for the third test was significantly higher. Major extensive damage was seen in JA-Plain-RF after testing. Some fragmentation and scabbing also occurred.

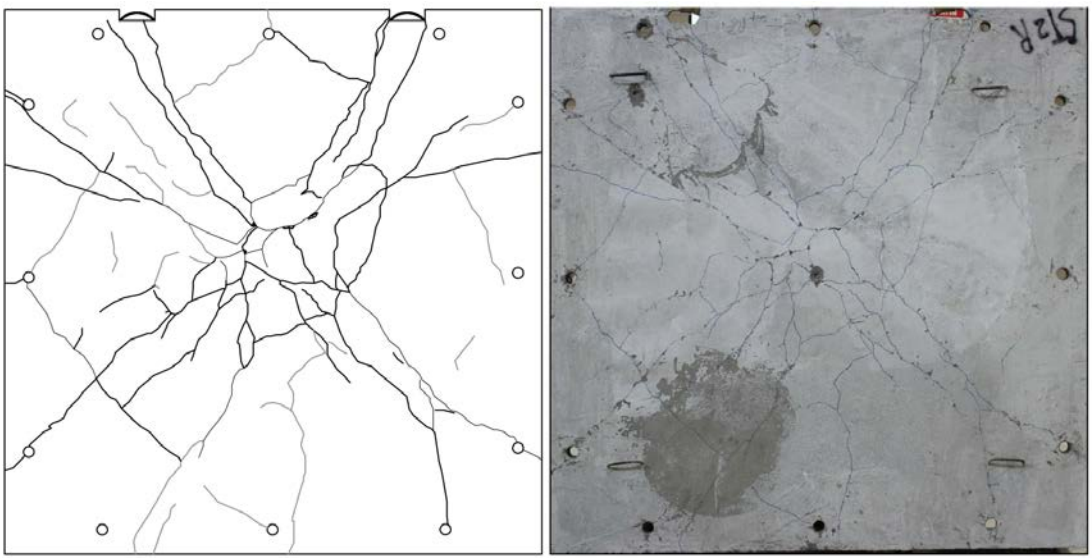

Figure 4.4.19. Front Face Crack Patterns After Testing for Panel JA2-075-RF

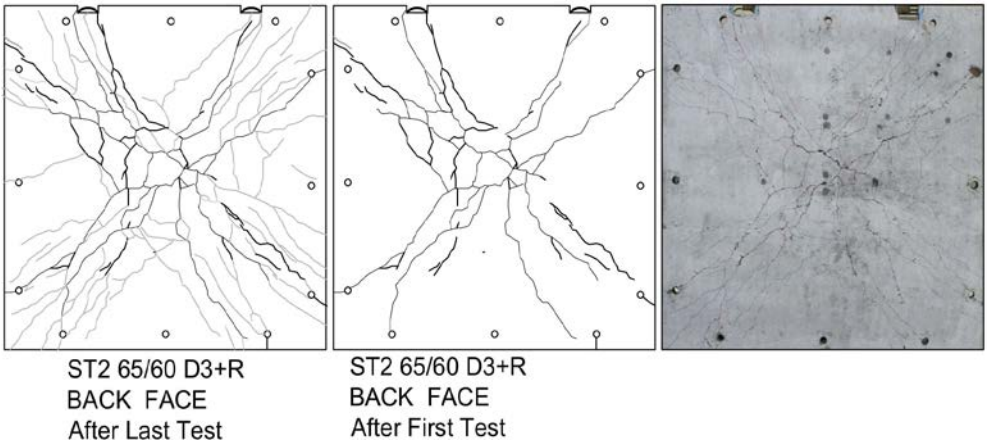

Figure 4.4.20. Rear Face Crack Patterns After Testing for Panel JA2-075-RF

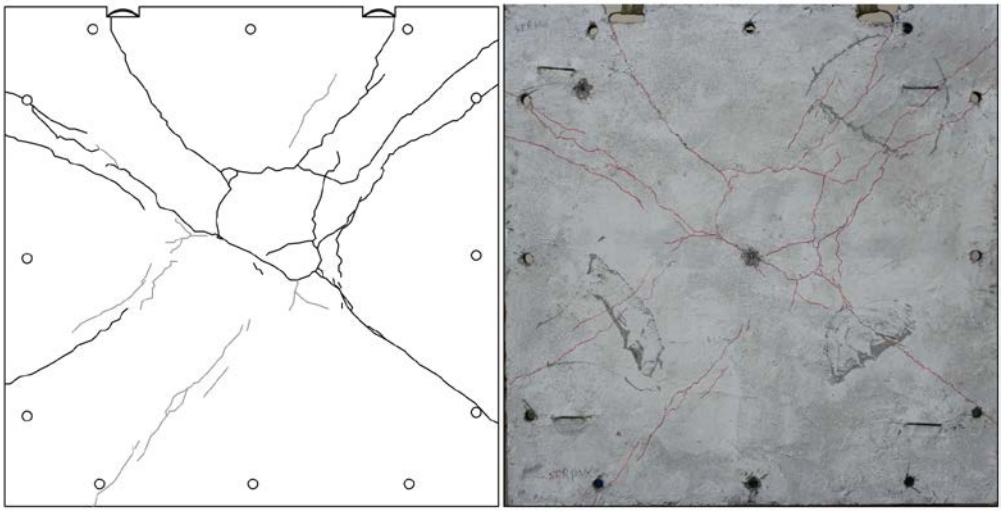

Figure 4.4.21. Front Face Crack Patterns After Testing for Panel JA2-075-RF+PVA

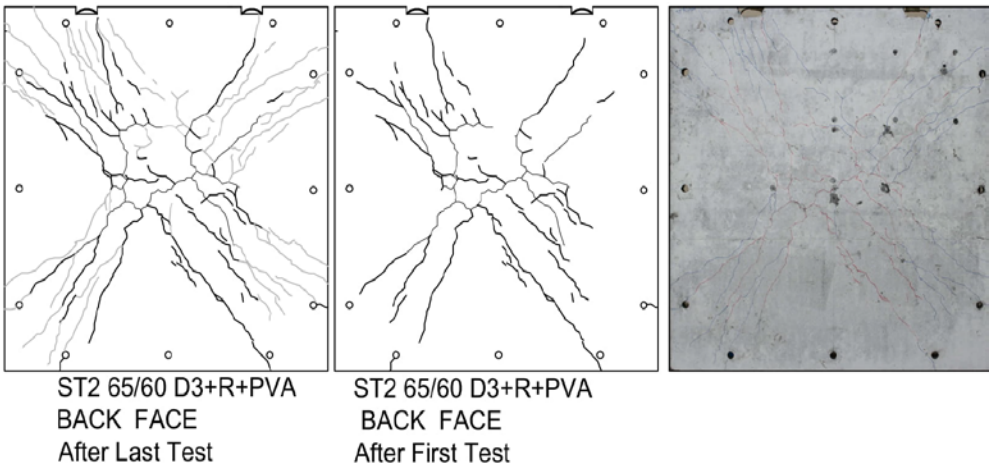

Figure 4.4.22. Rear Face Crack Patterns After Testing for Panel JA2-075-RF+PVA

Figure 4.4.23. Front Face Crack Patterns After Testing for Panel JA-Plain-RF

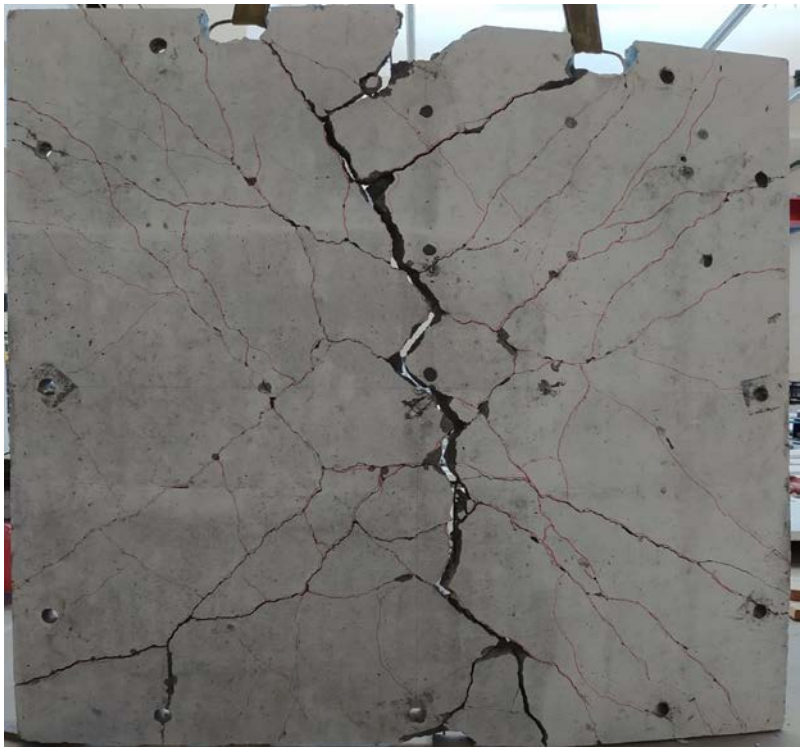

Figure 4.4.24. Rear Face Crack Patterns After Testing for Panel JA-Plain-RF

4.5. Evaluation of Test Results

Test program was successful both in applying a rarely used method for simulating blast loads in laboratory environment and in the evaluation of the behavior of fiber reinforced concrete panels. The shock tube manufactured for this test program was able to create a shock wave on the panel specimens with a form close to an ideal shock wave resulting from an air detonation. Reflected pressures and impulses were able to reach levels that were sufficient to enable the observation of the panels' performance. Considering that these pressure levels were obtained with only a 5 bar driver pressure and driver pressures may be increased up to 11-12 bar levels, it can be seen that much higher pressure and impulse levels may be obtained and higher strength panels may be tested using this shock tube. On the other hand, it was seen that even identical driver pressure levels may create different reflected pressure and impulse on the specimens. This may create a problem when behavior observed from different panels need to be compared, since testing conditions cannot be kept identical. It is known that similar problems can be encountered in actual blast tests performed with real explosives as well. Nevertheless, although not identical, reflected pressures and impulses were mostly in the same order for identical driver pressures, so a comparative evaluation was still possible.

When all test results are evaluated, it is seen that steel fiber type and ratio played a dominant role in the blast behavior of the panels. The highest damage level was observed in the specimens containing the 35 mm shorter fibers in JA1-075 and JA1-075+PVA. Addition of PVA fibers did not make a significant contribution for these specimens either. On the other hand, a lower damage level was noted in specimens containing 60 mm longer fibers. In general, addition of PVA fibers had a positive effect on limiting crack widths and decreasing number of cracks in all HyFRC specimens compared to their SFRC counterparts. This positive effect remained unchanged even if the maximum displacement obtained from both tests was very close. Crack control was more effective in HyFRC specimens. It has to be noted that the shock wave also created a dynamic suction pressure, loading the panels in both directions. As a result, same cracks were observed on both the front and back face of the specimens. Therefore, the panels without ordinary steel reinforcement had a higher cracking and fragmentation potential when exposed to the blast load. In this respect, better crack control in HyFRC panels is of particular importance.

When maximum displacements for first tests are compared, specimens with 1.25% of 60 mm 3D single hook steel fibers (JA2-125) displayed the best performance. This shows that steel fiber ratio was dominant on panels' behavior. The specimens with 0.75 % of 60 mm 5D double hook steel fibers, JA3-075 and JA3-075+PVA, had a lower displacement at the midpoint and narrower cracks were developed when compared to JA2-075 and JA2-075+PVA specimens. The better mechanical anchorage provided by 5D steel fibers improved the performance of panels under blast loads. The specimen with perlite, JA2-075-Perlite+PVA, displayed a similar performance under blast loads compared to its counterpart without perlite, JA2-075+PVA, for the first two tests. This shows that replacing some of the fine aggregate with perlite can be a suitable solution in order to obtain lighter panels without affecting the strength.

Among all specimens, the specimens with fiber and ordinary steel reinforcement presented the lowest displacements and showed lowest levels of damage. Even after being tested three times, JA2-075-RF+PVA had a limited crack development compared to other specimens. The steel reinforcing mesh used was 5 mm bars with 150 mm spacing, providing a 0.0026 reinforcement ratio, which can be considered as a low ratio. Therefore, it is seen that even such a low ratio had a significant benefit in terms of blast resistance. Steel mesh used with fibers not only increased the strength of the panels, but also it helped limiting the number and widths of cracks, controlling the fragmentation. On the other hand, it should be noted that steel mesh without any fibers (JA-Plain-RF), did not show a good performance. The panel displayed extensive cracking and fragmentation after the tests. Therefore, it can be said that steel mesh by itself is not as effective in the blast performance without fibers in concrete.

CHAPTER 5

CONCLUSIONS

Within the scope of the study, 13 panels of 1900x1900x50 mm dimensions were cast with various fiber concrete mixtures and they were tested under blast loads. Blast loads were given to the panels through a specially designed and manufactured shock tube.

When the results obtained are examined, it is seen that the fiber addition provides a significant ductility to the concrete under blast loads. This effect is valid for both steel fiber reinforced concrete and hybrid fiber reinforced concrete in which steel and PVA fiber are used together. The positive effect of the use of hybrid fiber reinforced concrete on the behavior was observed very clearly. All hybrid fiber reinforced panels developed much more controlled, more numerous but much narrower cracks than their steel fiber reinforced counterparts. This played an important role both in maintaining the integrity of the panel in an overload like explosion and in resisting higher explosion impulses of the panels.

The use of steel reinforcement with fibers contributed positively to the behavior of the panels under blast loads. In addition to the increase in strength, the steel reinforcement allowed better crack control and a more ductile behavior. The best results were obtained with hybrid fiber steel reinforced panels.

It was observed that the type of steel fiber used in the behavior of hybrid fiber reinforced concrete panels greatly affects the behavior. For example, the presence or absence of PVA fibers in panels using 35 mm short steel fibers did not change the behavior much in shock tube tests. On the other hand, there were significant differences between hybrid fiber reinforced concrete and concrete using only steel fiber in panels with 60 mm longer steel fibers. This situation reveals that for fiber hybridization to be effective, longer steel fibers must also be able to work effectively. The larger difference between steel fiber-only concrete and hybrid fiber reinforced concrete in double hook 5D fibers supports this conclusion. The shorter 35 mm steel fibers are less effective in controlling macro cracks, and the presence of PVA fibers that are effective on micro cracks cannot fill this gap.

Replacing some of the fine aggregate with perlite, a weak aggregate type, did not result in a worse behavior in shock tube experiments. Although this is promising for obtaining lighter panels, more work is needed in this regard.

REFERENCES

Abadel, A., Al-Salloum, Y., Abbas, H., Siddiqui, N., Almusallam, T. 2016. "Mechanical properties of hybrid fibre-reinforced concrete – analytical modelling and experimental behaviour", Magazine of Concrete Research, 68(16), 823-843.

American Concrete Institute. 2014. 370R-14: Report for the Design of Concrete Structures for Blast Effects. USA.

Baker, W. E., 1973, "Explosions in Air", University of Texas Press.

Betterman, L. R., Ouyang, C., Shah, S. P. 1995. "Fiber-Matrix Interaction in Microfiber-Reinforced Mortar", Advanced Cement Based Materials, 2(3), 53-61.

Bewick, B. T., Salim, H. A., Hoemann, J. 2008. Prefabricated Tilt-up Concrete Panels for Blast Resistant Design. Philadelphia PA: 78th Shock and Vibration Symposium.

Cadoni, E., Drdlová, M., Čechmánek, R., Řídký, R. 2015. "Blast impact behaviour of concrete with different fibre reinforcement", EPJ Web of Conferences, 94, 05006.

Carriere, M., Heffernan, P. J., Wight, R. G., Braimah, A. 2009. "Behaviour of steel reinforced polymer (SRP) strengthened RC members under blast load", Canadian Journal of Civil Engineering, 36(8), 1356-1365.

Castedo, R., Segarra, P., Alanon, A., Lopez, L. M., Santos, A. P., Sanchidrian, J. A. 2015. "Air blast resistance of full-scale slabs with different compositions: Numerical modeling and field validation", International Journal of Impact Engineering, 86, 145-156.

Chasioti, S. G., Vecchio, F. J. 2017. "Effect of Fiber Hybridization on Basic Mechanical Properties of Concrete", ACI Materials Journal, 114(3), 375-384.

Chopra, A. K. 1995. Dynamics of Structures – Theory and applications to earthquake engineering. (International Edition). USA: Prentice Hall.

Çetin, F. Ş. 2020. "Mechanical Behavior of Hybrid Fiber Reinforced Concrete Under Direct Tension", Yüksek Lisans Tezi, İzmir Yüksek Teknoloji Enstitüsü, Mühendislik ve Fen Bilimleri Enstitüsü, İnşaat Mühendisliği ABD, 78 sayfa, İzmir.

Department of Defence, 2008. UFC 3-340-02: Structures to Resist the Effects of Accidental Explosions. USA.

Drdlova, M., Buchar, J., Ridky, R., Kratky, J. 2015. "Blast resistance characteristics of concrete with different types of fibre reinforcement", Structural Concrete, 16(4), 508-517.

Enfedaque, A., Cendon, D., Galvez, F., Sanchez-Galvez, V. 2011. "Failure and impact behavior of facade panels made of glass fiber reinforced cement(GRC)", Engineering Failure Analysis, 18(7), 1652-1663.

Institution of Civil Engineers. 1995. Blast Effects on Buildings. London: Thomas Telford Publications.

FEMA. 2003. FEMA 426-Reference Manual to Mitigate Potential Terrorist Attacks Against Buildings.

Foglar, M., Kovar, M. 2014. “Blast Reinforcement of FRC Specimens with Steel Fibers of Low Ductility”, Engineering Mechanics 2014, 176-179.

Haido, J. H., Abu Bakar, B. H., Abdul-Razzak, A. A., Jayaprakash, J., Choong, K. K. 2011. “Simulation of dynamic response for steel fibrous concrete members using new material modeling”, Construction and Building Materials, 25(3), 1407-1418.

Lan, S. R., Lok, T. S., Heng, L. 2005. “Composite structural panels subjected to explosive loading”, Construction and Building Materials, 19(5), 387-395.

Li, J., Wu, C. Q., Hao, H. 2015. “An experimental and numerical study of reinforced ultra-high performance concrete slabs under blast loads”, Materials & Design, 82, 64-76.

Lloyd, A. 2010. Performance of Reinforced Concrete Columns under Shock Tube Induced Shock Wave Loading (M.A.Sc.). Ottawa: University of Ottawa.

Mao, L., Barnett, S., Begg, D., Schleyer, G., Wight, G. 2014. “Numerical simulation of ultra high performance fibre reinforced concrete panel subjected to blast loading”, International Journal of Impact Engineering, 64, 91-100.

Millard, S. G., Molyneaux, T. C. K., Barnett, S. J., Gao, X. 2010. “Dynamic enhancement of blast-resistant ultra high performance fibre-reinforced concrete under flexural and shear loading”, International Journal of Impact Engineering, 37(4), 405-413.

Mohammed Alias Yusof*1 , Norazman2 , Ariffin3 , Fauzi Mohd Zain4 , Risby5 , CP Ng6. 2010. “Normal Strength Steel Fiber Reinforced Concrete Subjected to Explosive Loading”, International Journal of Sustainable Construction Engineering & Technology.

Oswald, C. J., Bazan, M. 2014. “Performance and Blast Design for Non-Load Bearing Precast Concrete Panels”, Structures Congress 2014, 143-154.

Oswald, C. J., Moriarty, C. W. 2014. “Blast-resistant architectural precast concrete cladding for government buildings”, Pci Journal, Summer, 36-42.

Razaqpur, A. G., Contestabile, E., Tolba, A. 2009. “Experimental study of the strength and deformations of carbon fibre reinforced polymer (CFRP) retrofitted reinforced concrete slabs under blast load”, Canadian Journal of Civil Engineering, 36(8), 1366-1377.

Razaqpur, A. G., Tolba, A., Contestabile, E. 2007. “Blast loading response of reinforced concrete panels reinforced with externally bonded GFRP laminates”, Composites Part B-Engineering, 38(5-6), 535-546.

Şahmaran M., Yaman I. O. 2007. “Hybrid fiber reinforced self-compacting concrete with high-volume coarse fly ash”, Concr. Build. Mater., 21, 150-156.

Tanapornraweekit, G., Haritos, N., Mendis, P. 2011. “Behavior of FRP-RC Slabs under Multiple Independent Air Blasts”, Journal of Performance of Constructed Facilities, 25(5), 433-440.

Tadepalli, P., Mo, Y., Hsu, T., & Vogel, J. (2009). Mechanical Properties of Steel Fiber Reinforced Concrete Beams. 2009 Structures Congress (pp. 1039-1048). Austin, TX: ASCE.

The Scientific and Technological Research Council of Turkey (TUBITAK) 112M822. 2013-2015. Çelik fiber katkısının darbe yüküne maruz kalan betonarme elemanların dayanımına olan etkileri. Advisor: Selçuk Saatcı, Researcher: Tahir Kemal Erdem. Completed.

The Scientific and Technological Research Council of Turkey (TUBITAK) 115M296. 2015-2017. Yüksek enerji yutma kapasitesine sahip çimento esaslı kompozit geliştirilmesi ve yeni nesil beton otokorkuluk üretimine uygulanması. Advisor: Tahir Kemal Erdem, Researcher: Selçuk Saatcı. Completed.

U.S. Army Corps of Engineers. 2008. PDC-TR 06-08-Single Degree of Freedom Structural Response Limits for Antiterrorism Design. USA.

Wang, W., Zhang, D., Lu, F. Y., Wang, S. C., Tang, F. J. 2013. “Experimental study and numerical simulation of the damage mode of a square reinforced concrete slab under close-in explosion”, Engineering Failure Analysis, 27, 41-51.

Wu, C. Q., Huang, L., Oehlers, D. J. 2011. “Blast Testing of Aluminum Foam-Protected Reinforced Concrete Slabs”, Journal of Performance of Constructed Facilities, 25(5), 464-474.

Yamaguchi, M., Murakami, K., Takeda, K., Mitsui, Y. 2011. “Blast Resistance of Polyethylene Fiber Reinforced Concrete to Contact Detonation”, Journal of Advanced Concrete Technology, 9(1), 63-71.

Yoo, D. Y., Banthia, N. 2017. “Mechanical and structural behaviors of ultra-high-performance fiber-reinforced concrete subjected to impact and blast”, Construction and Building Materials, 149, 416-431.

Zhang, J., Maalej, M., Quek, S. T. 2007. “Performance of hybrid-fiber ECC blast/shelter panels subjected to drop weight impact”, Journal of Materials in Civil Engineering, 19(10), 855-863.

Zhou, X. Q., Huang, X., Xia, Y. 2014. “Numerical Simulation of Fiber Reinforced Concrete Slab Subjected to Blast Loading”, 13th International Symposium on Structural Engineering, ISSE-13, 1987 – 1993.

APPENDIX A

TEST RESULTS

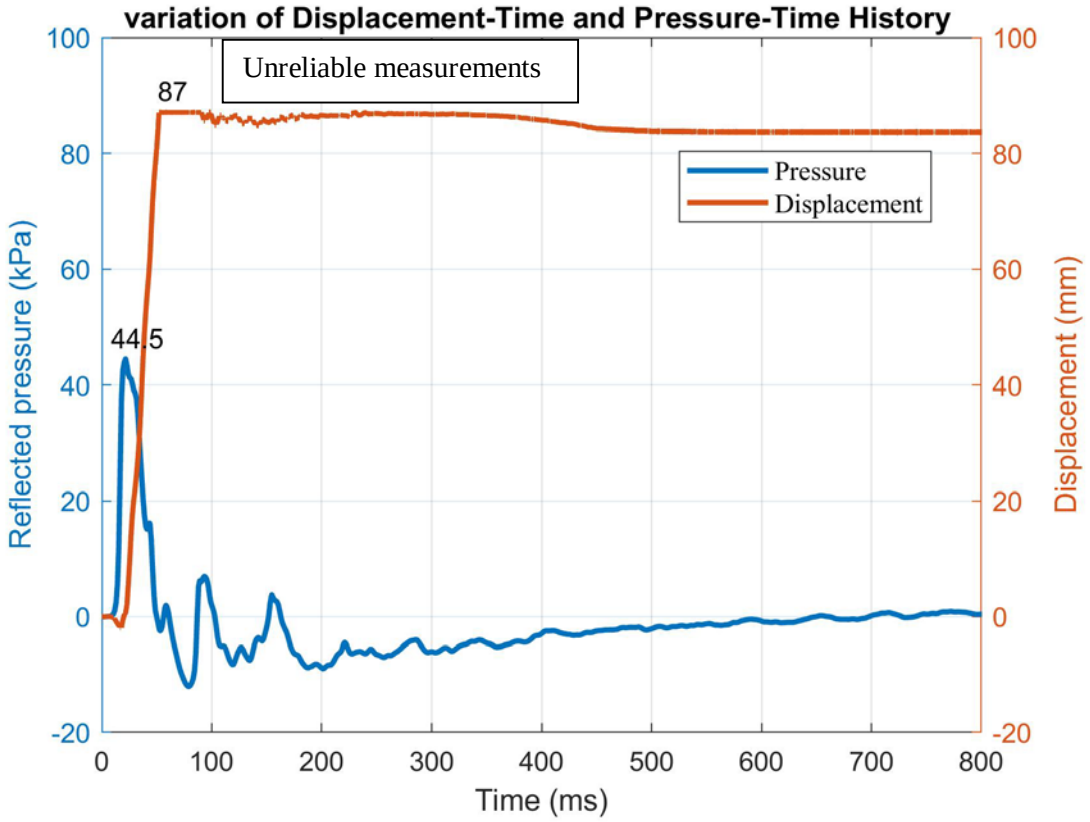

Figure A.1. Mid-span Panel Displacement and Pressure in Blast Test for JA1-075 Test-1

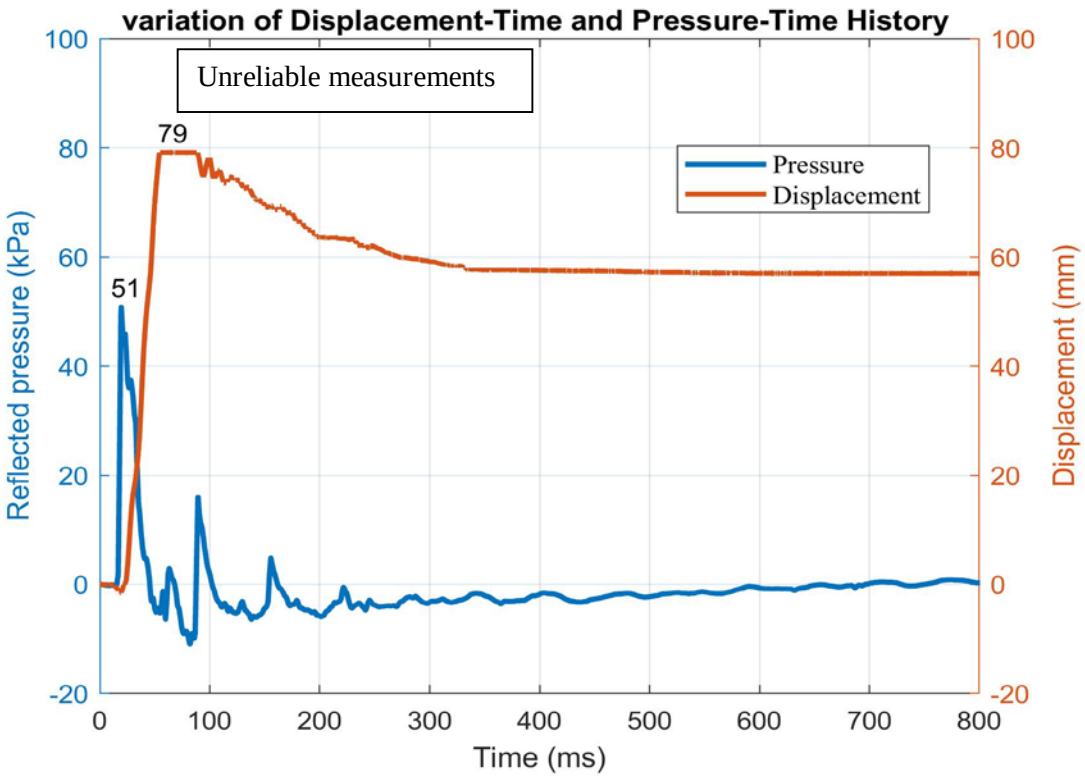

Figure A.2. Mid-span Panel Displacement and Pressure in Blast Test for JA1-075+PVA Test-1

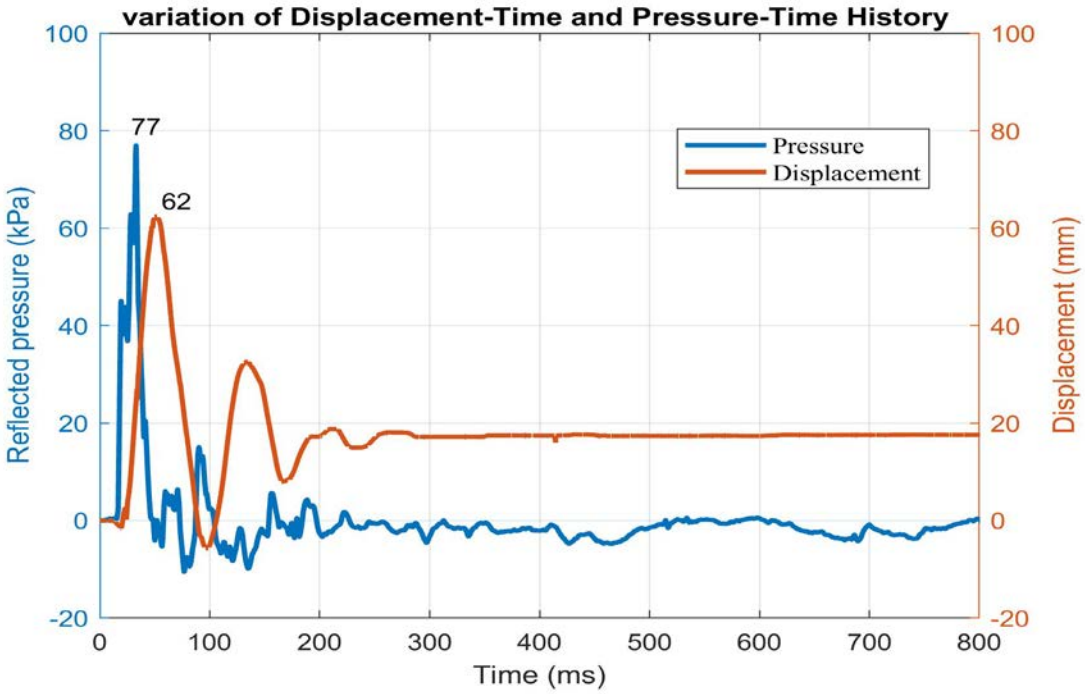

Figure A.3. Mid-span Panel Displacement and Pressure in Blast Test for JA2-075 Test-13

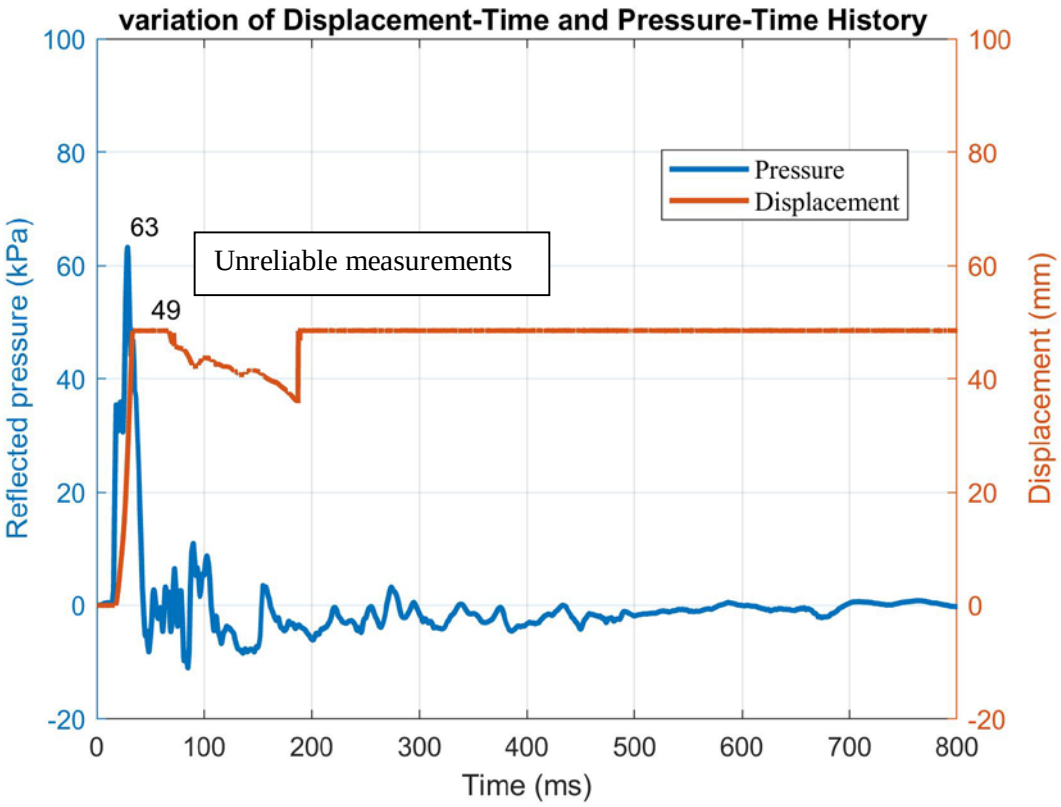

Figure A.4. Mid-span Panel Displacement and Pressure in Blast Test for JA2-075 Test-2

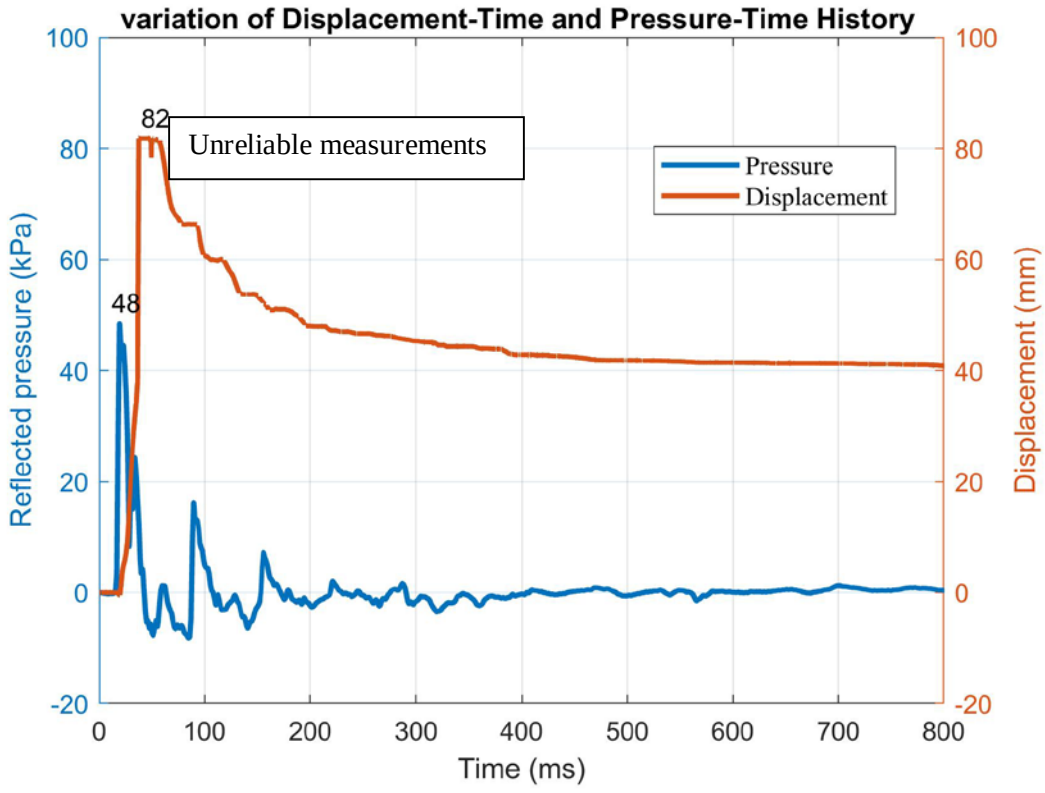

Figure A.5. Mid-span Panel Displacement and Pressure in Blast Test for JA2-075+PVA Test-1

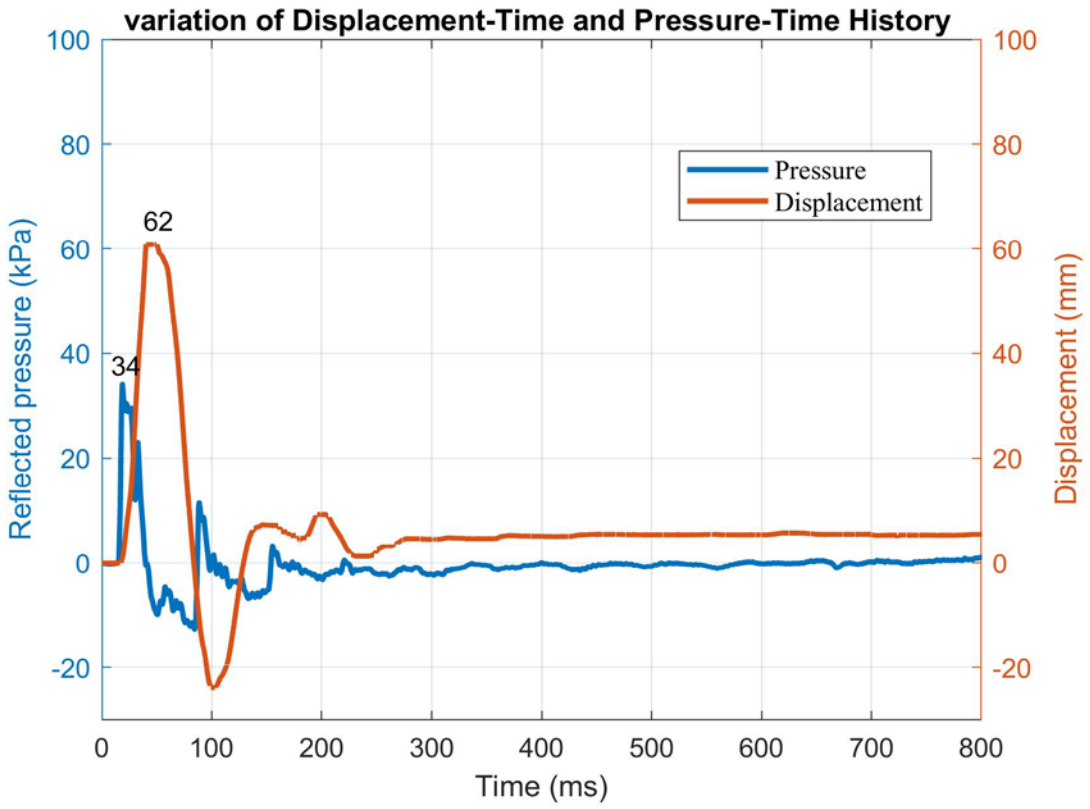

Figure A.6. Mid-span Panel Displacement and Pressure in Blast Test for JA2-075+PVA Test-2

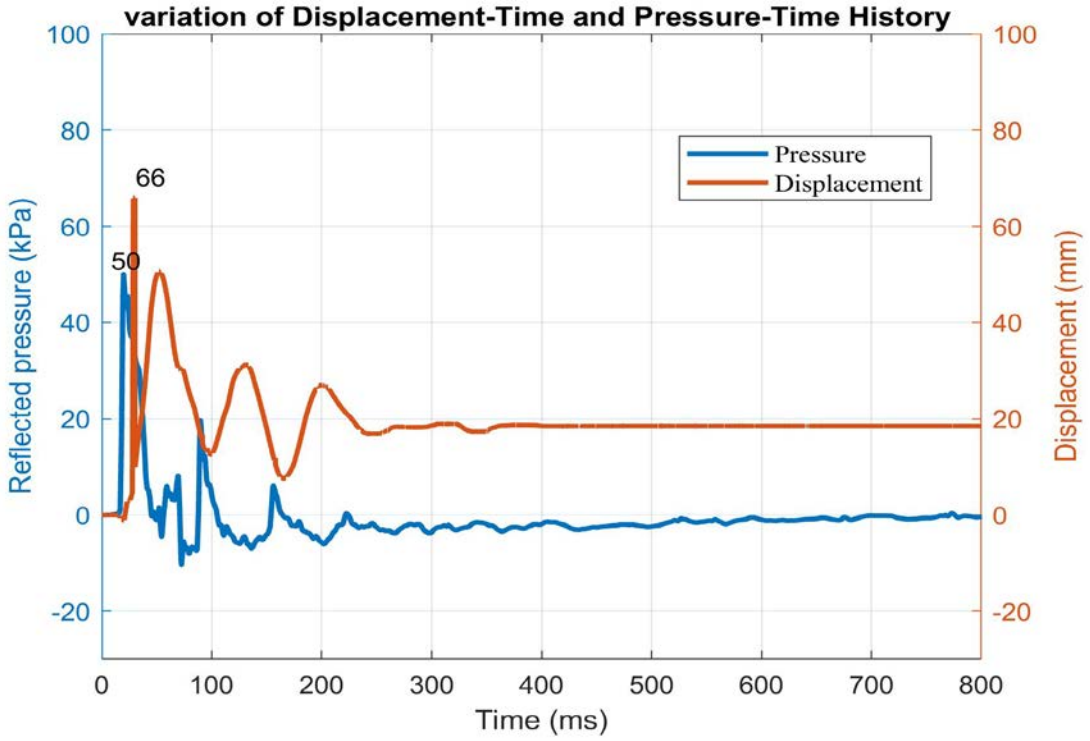

Figure A.7. Mid-span Panel Displacement and Pressure in Blast Test for JA2-075-perlite+PVA-Test-1

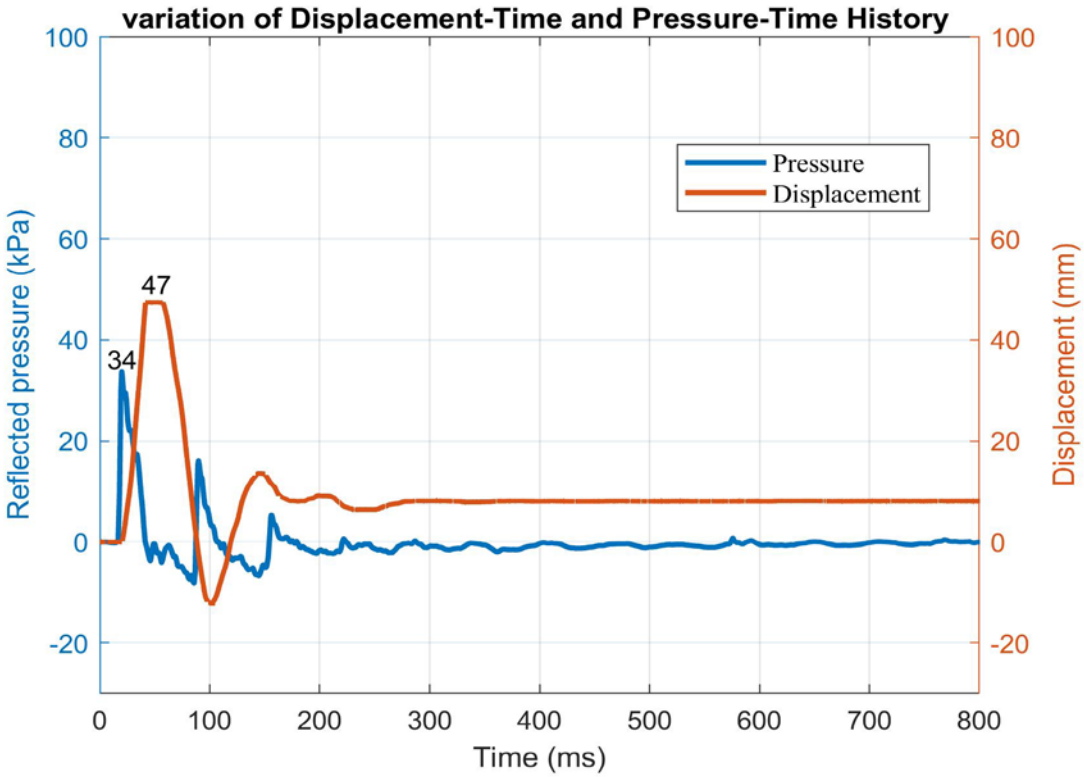

Figure A.8. Mid-span Panel Displacement and Pressure in Blast Test for JA2-075-perlite+PVA-Test-2

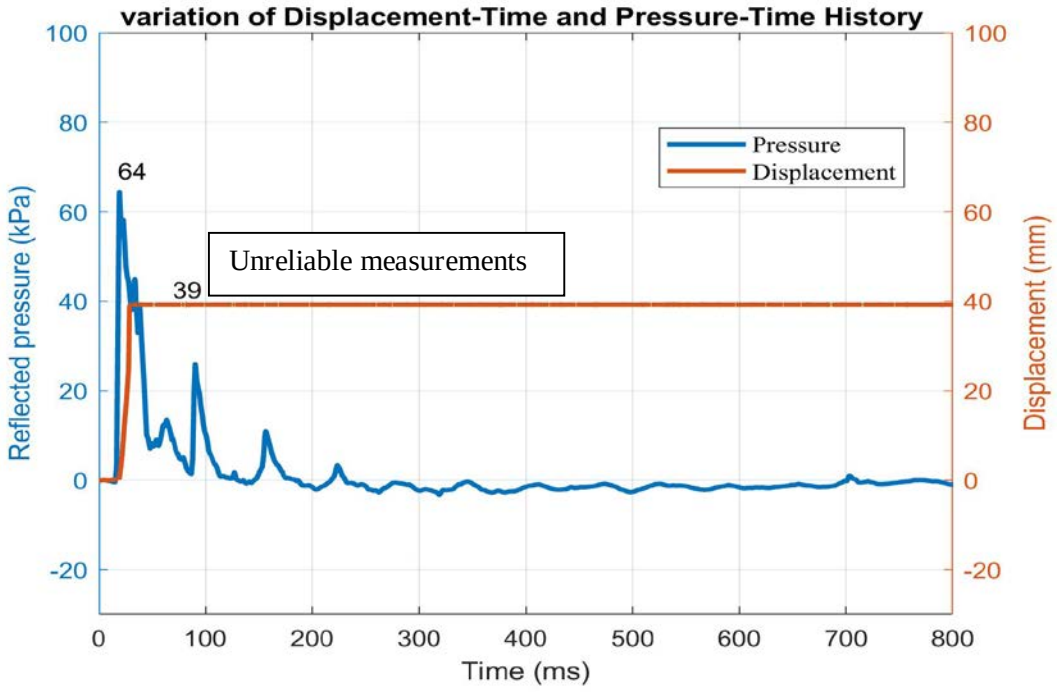

Figure A.9. Mid-span Panel Displacement and Pressure in Blast Test for JA2-075-perlite+PVA-Test-3

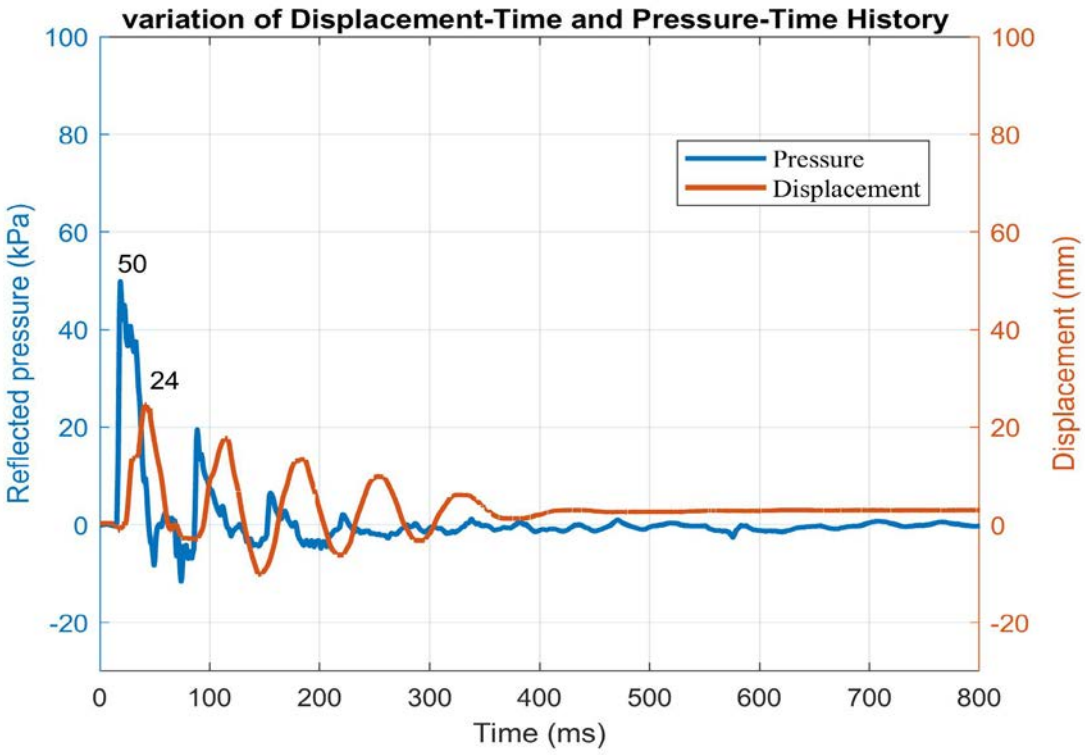

Figure A.10. Mid-span Panel Displacement and Pressure in Blast Test for JA2-075-RF Test-1

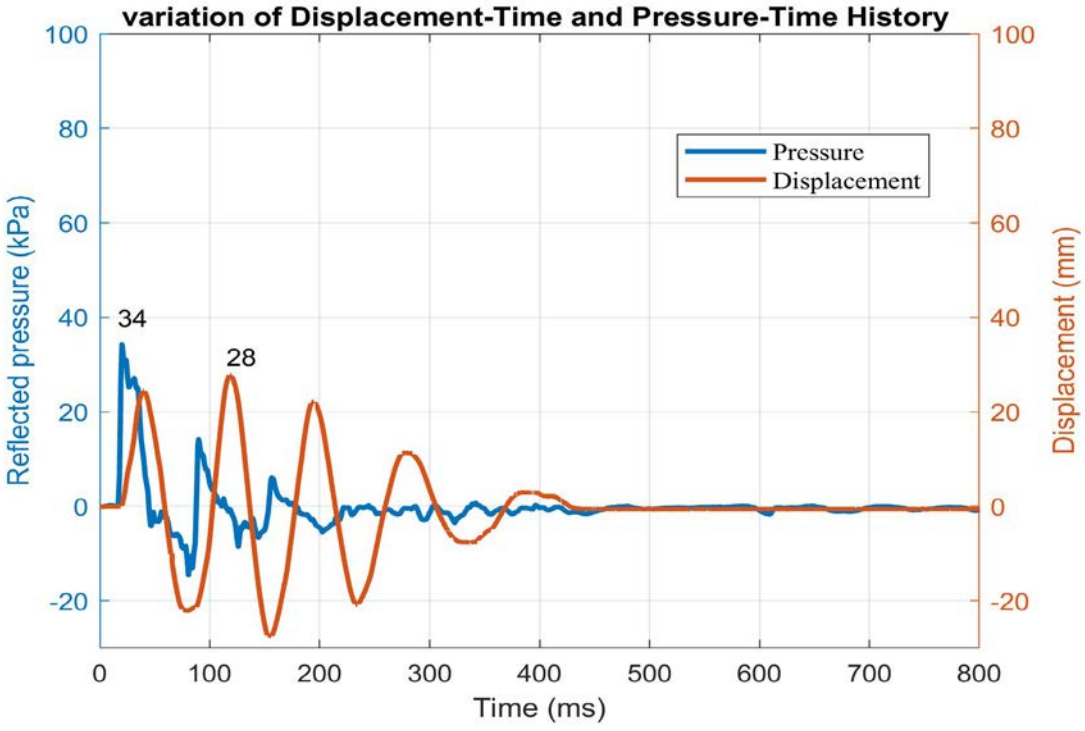

Figure A.11. Mid-span Panel Displacement and Pressure in Blast Test for JA2-075-RF Test-2

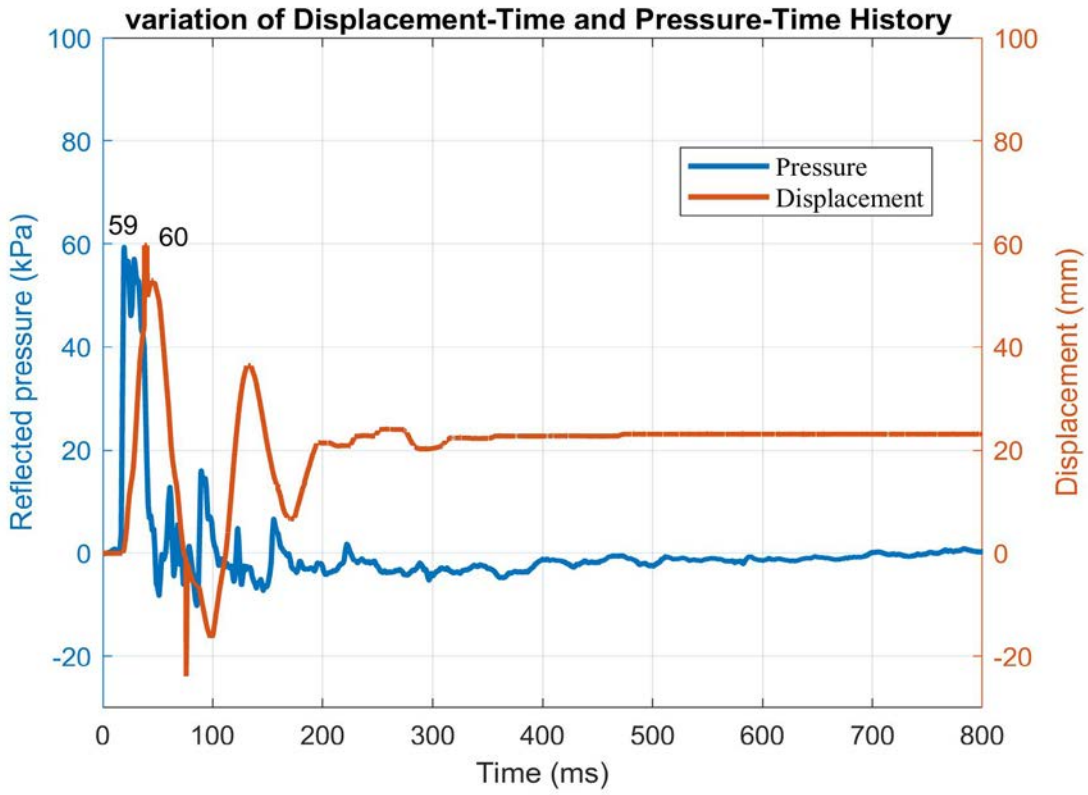

Figure A.12. Mid-span Panel Displacement and Pressure in Blast Test for JA2-075-RF Test-3

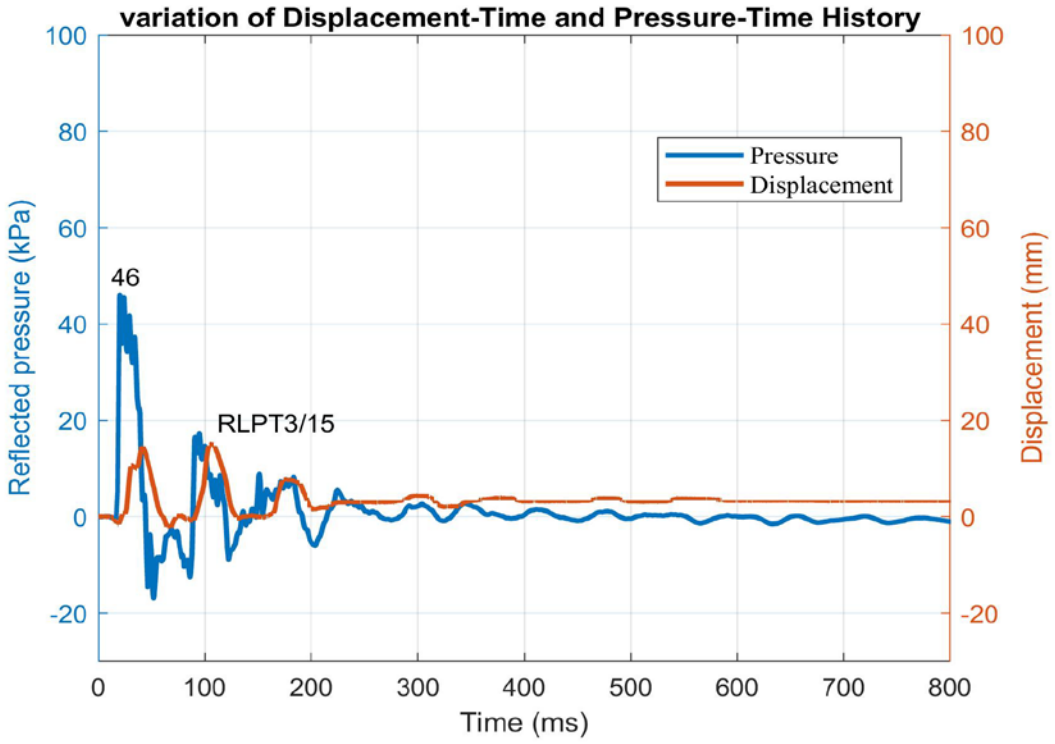

Figure A.13. Mid-span Panel Displacement and Pressure in Blast Test for JA2-075+PVA-RF-Test-1

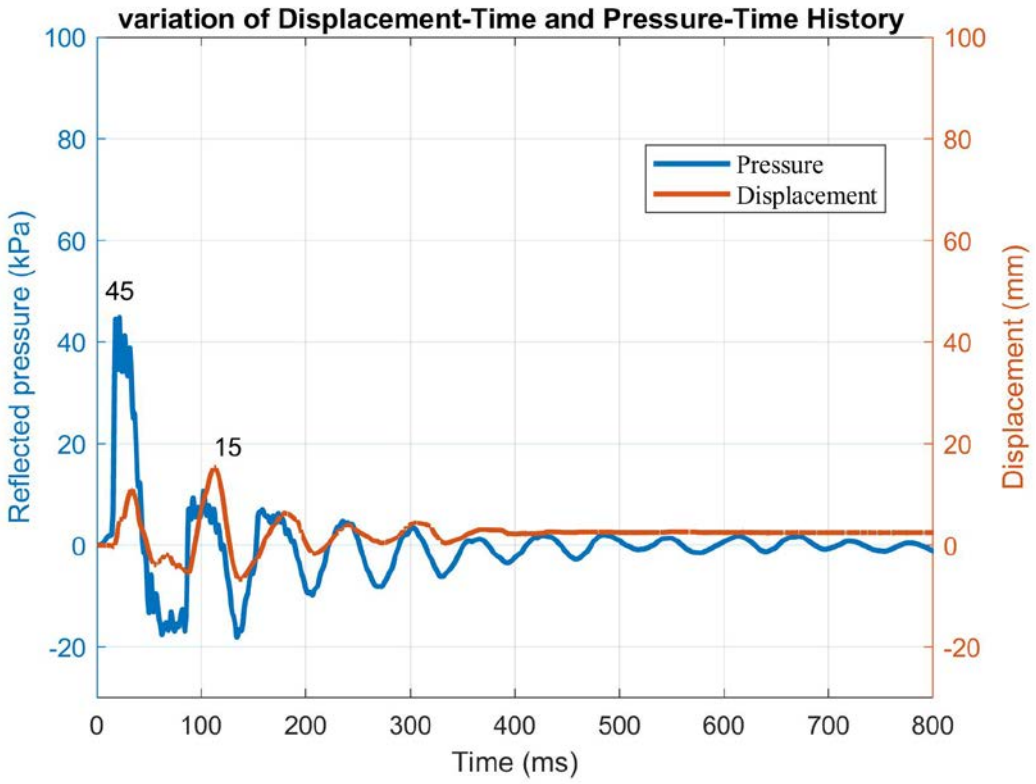

Figure A.14. Mid-span Panel Displacement and Pressure in Blast Test for JA2-075+PVA-RF-Test-2

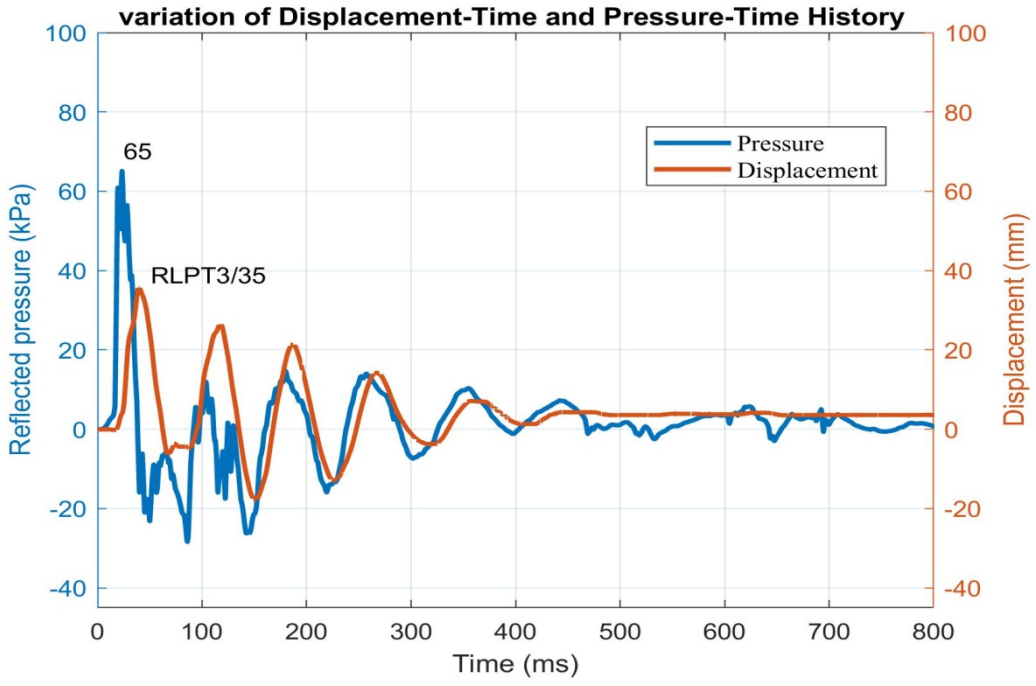

Figure A.15. Mid-span Panel Displacement and Pressure in Blast Test for JA2-075+PVA-RF-Test-3

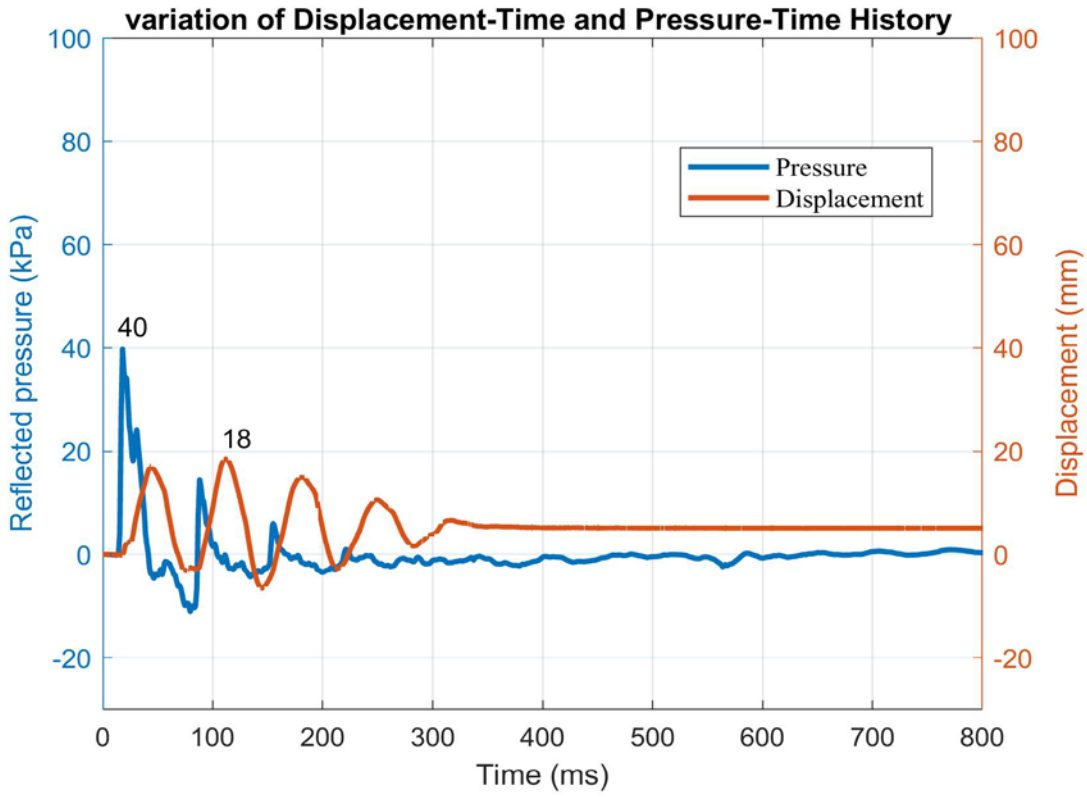

Figure A.16. Mid-span Panel Displacement and Pressure in Blast Test for JA2-125 Test-1

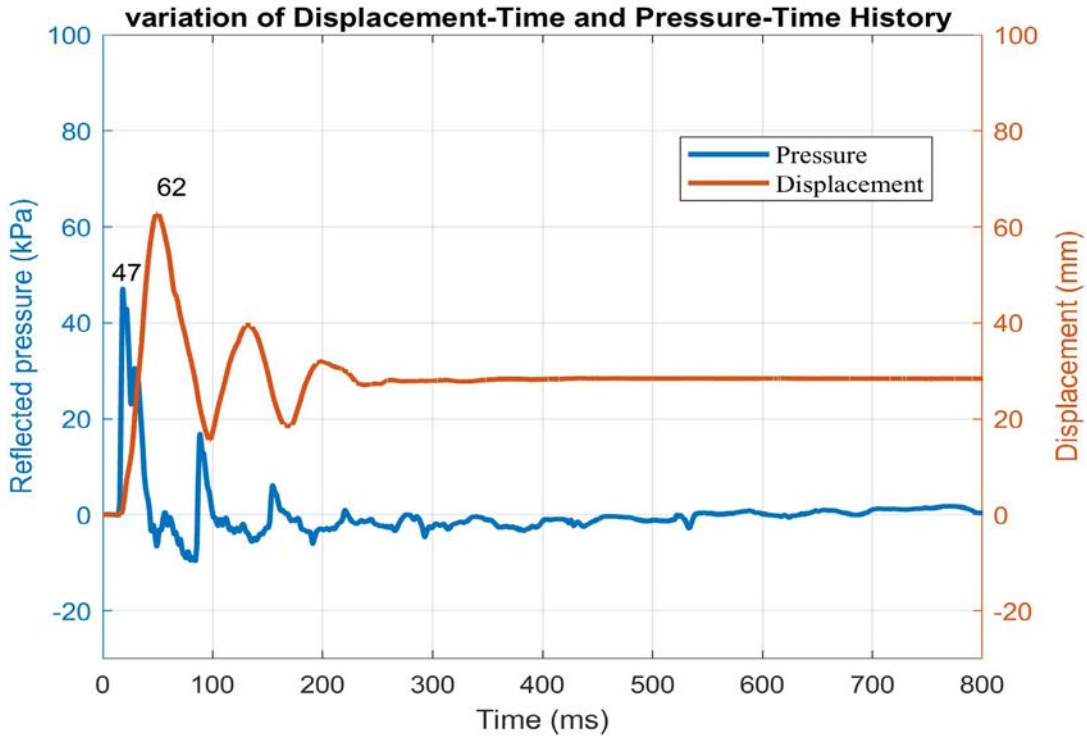

Figure A.17. Mid-span Panel Displacement and Pressure in Blast Test for JA2-125 Test-2

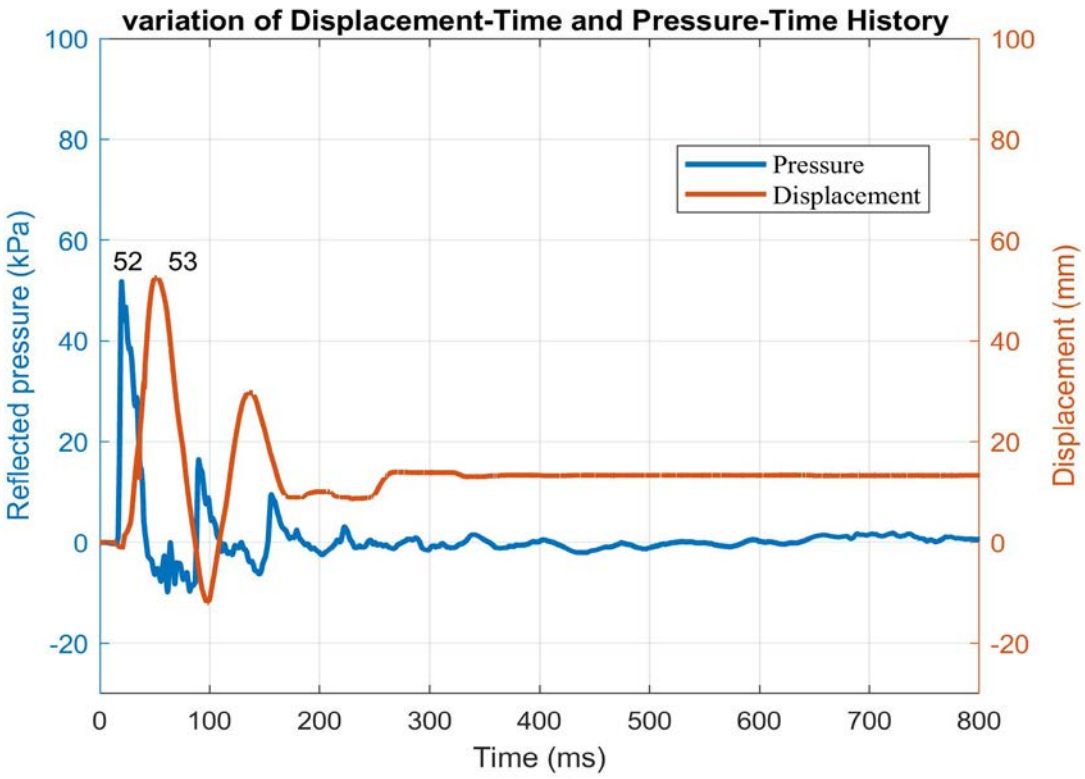

Figure A.18. Mid-span Panel Displacement and Pressure in Blast Test for JA2-125 +PVA Test1

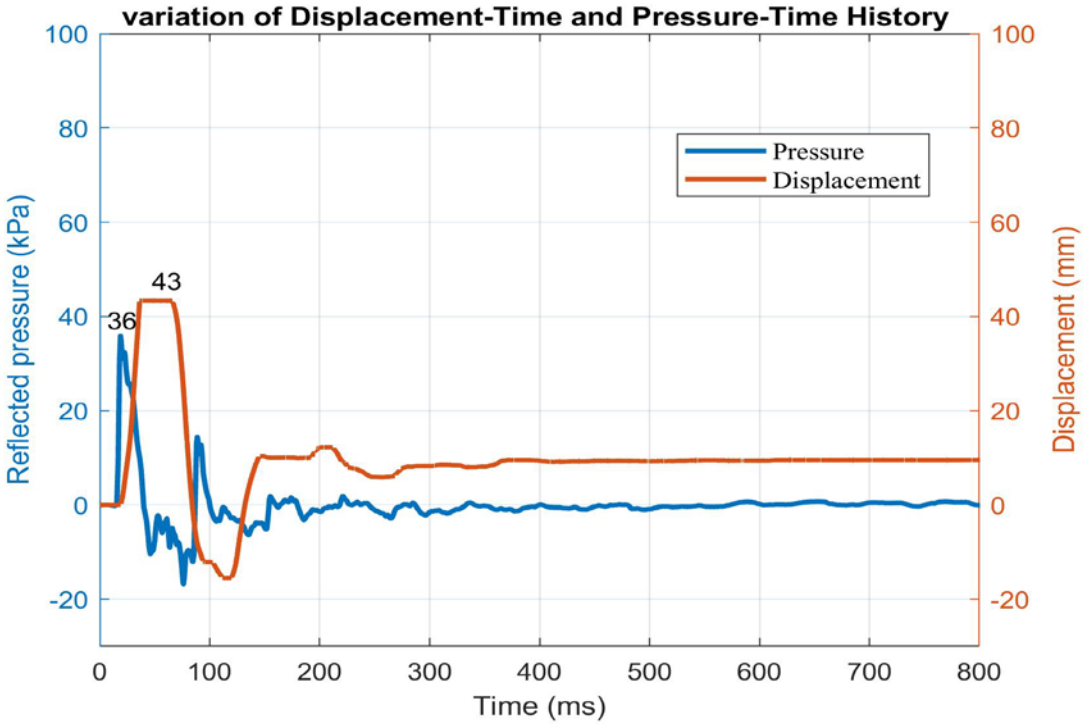

Figure A.19. Mid-span Panel Displacement and Pressure in Blast Test for JA2-125 +PVA Test-2

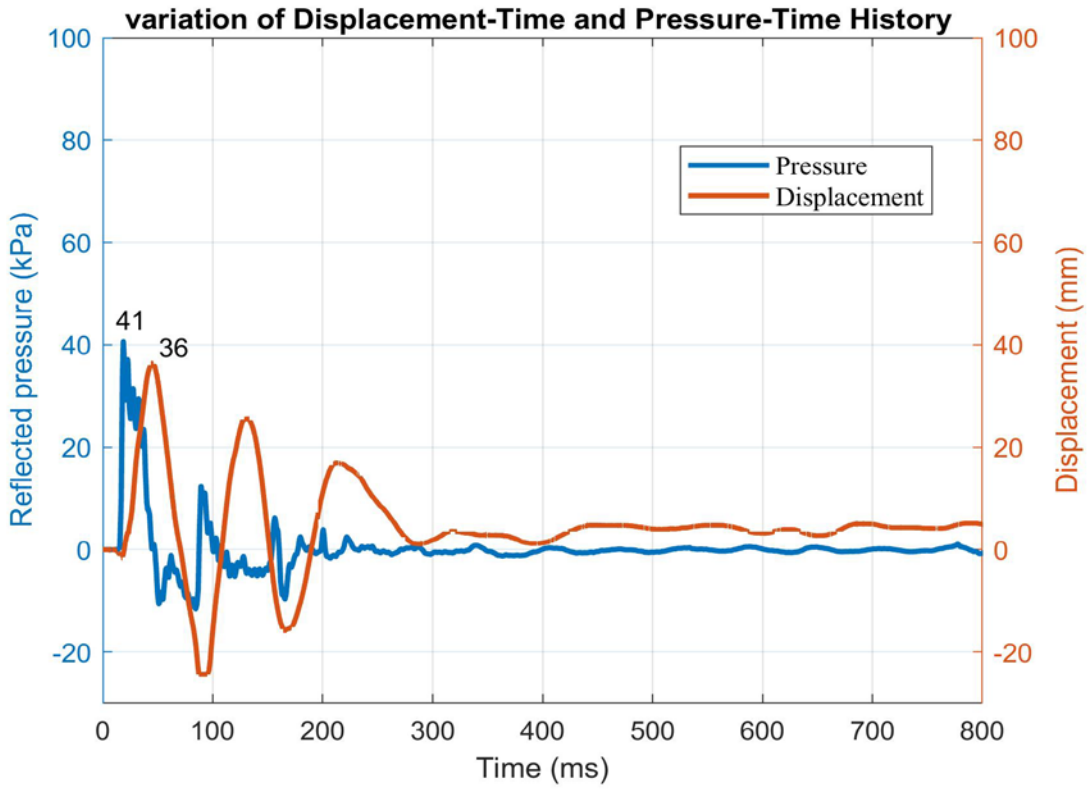

Figure A.20. Mid-span Panel Displacement and Pressure in Blast Test for JA3-075 Test-1

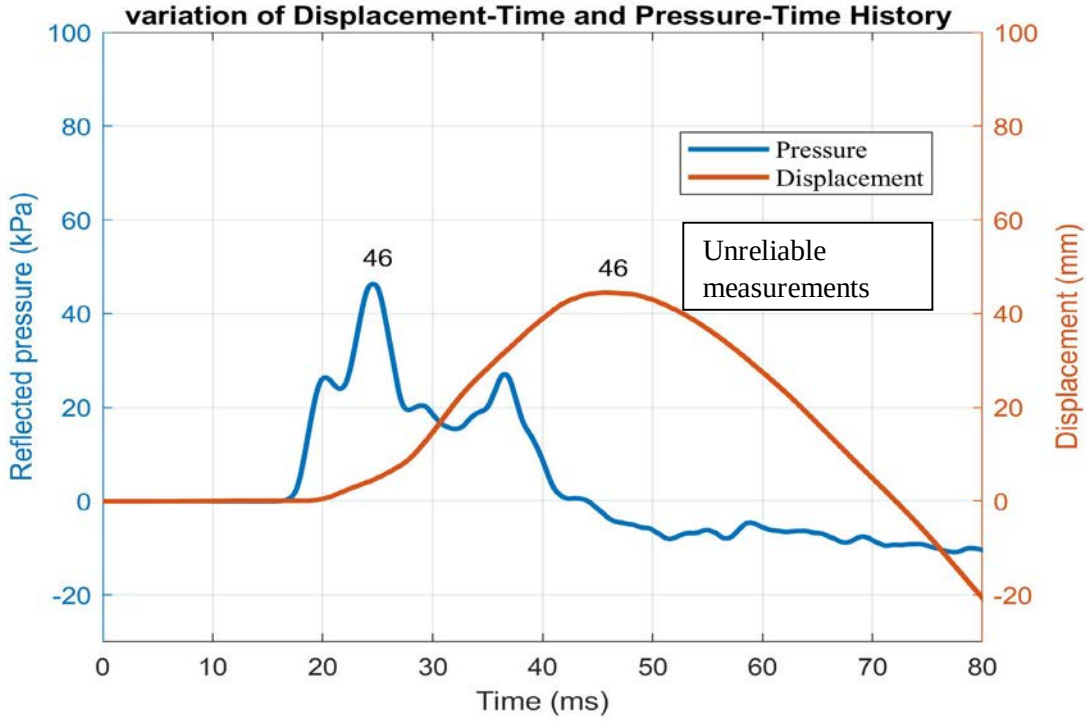

Figure A.21. Mid-span Panel Displacement and Pressure in Blast Test for JA3-075 Test-2

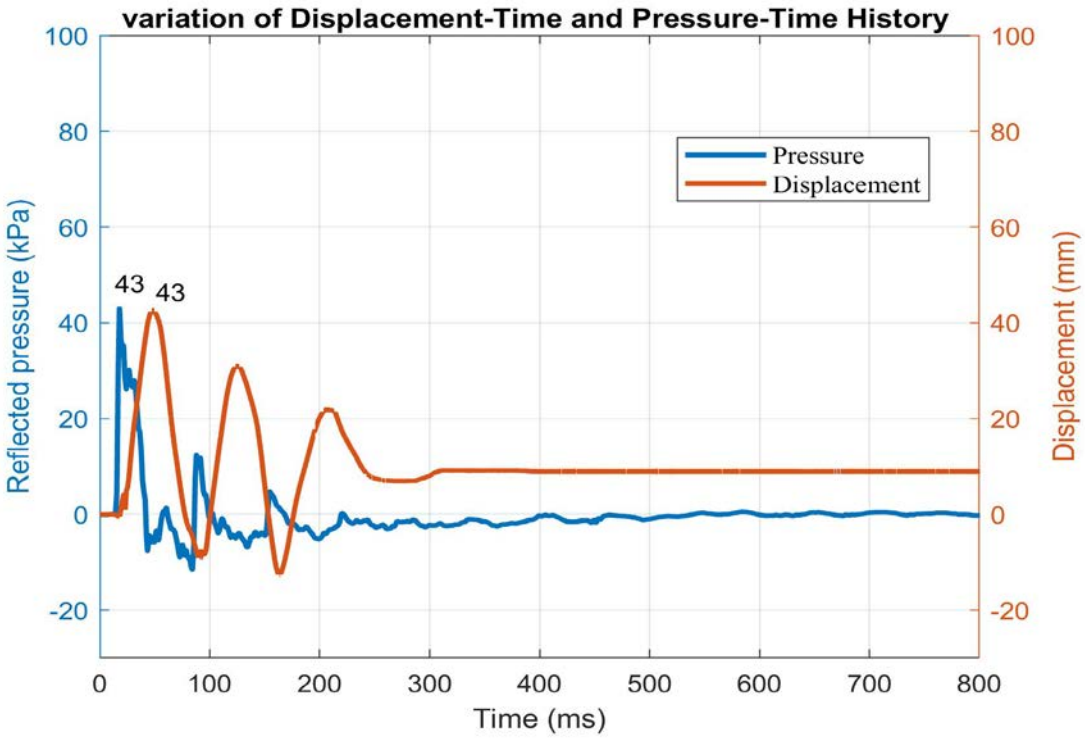

Figure A.22. Mid-span Panel Displacement and Pressure in Blast Test for JA3-075+PVA Test-1

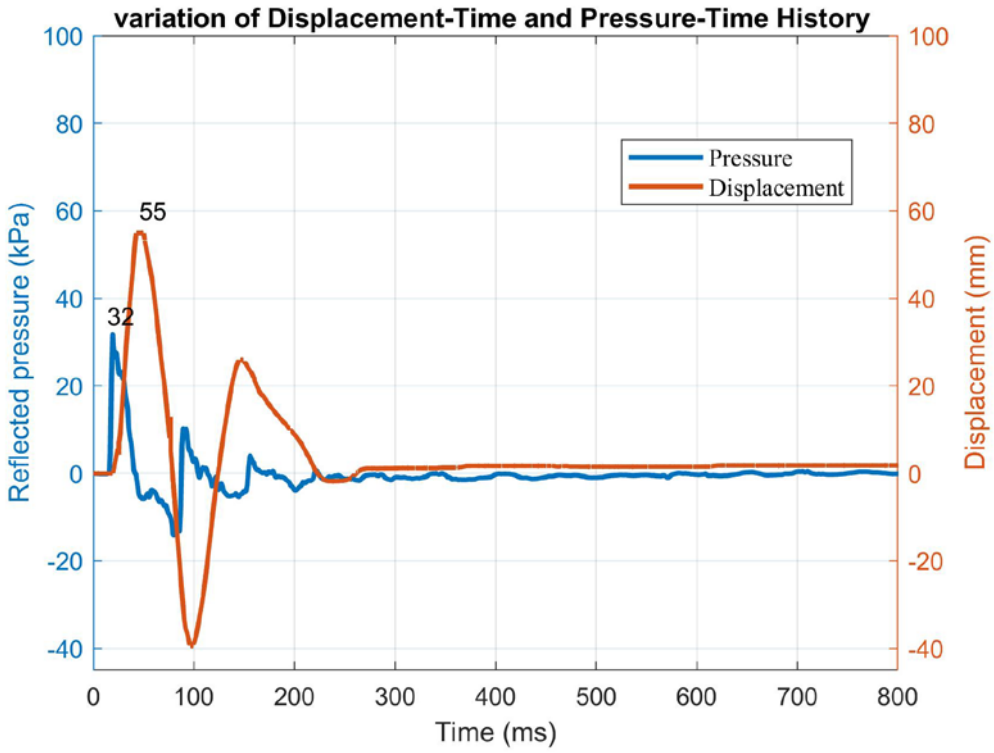

Figure A.23. Mid-span Panel Displacement and Pressure in Blast Test for JA3-075+PVA Test-2

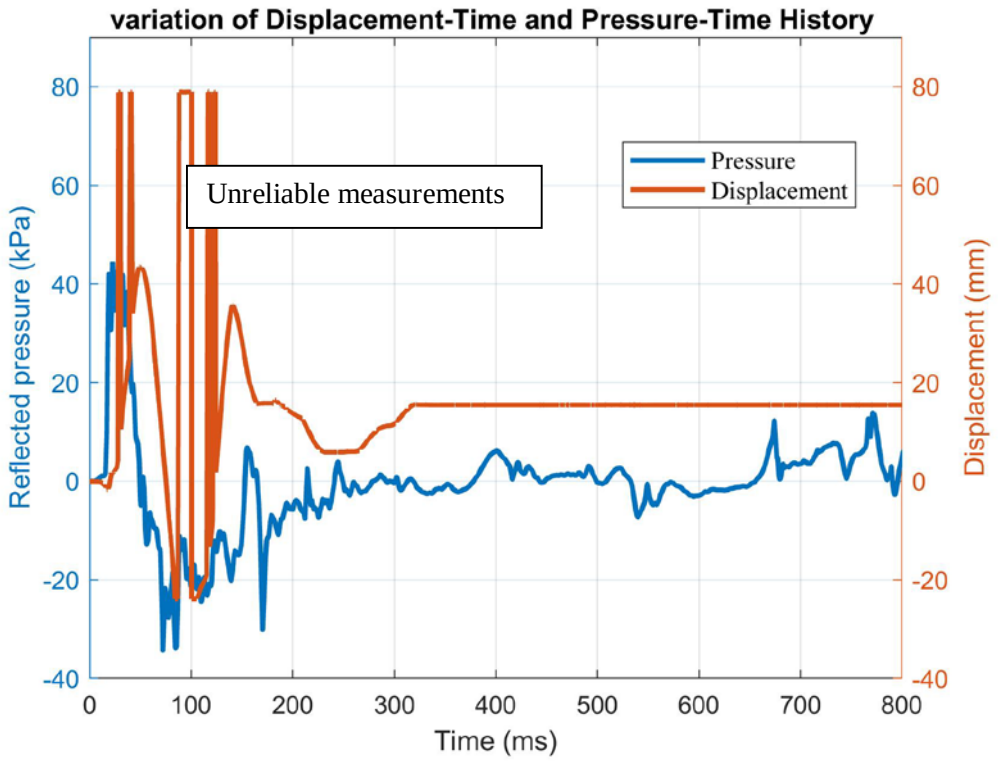

Figure A.24. Mid-span Panel Displacement and Pressure in Blast Test for JA-Plain-RF Test-1

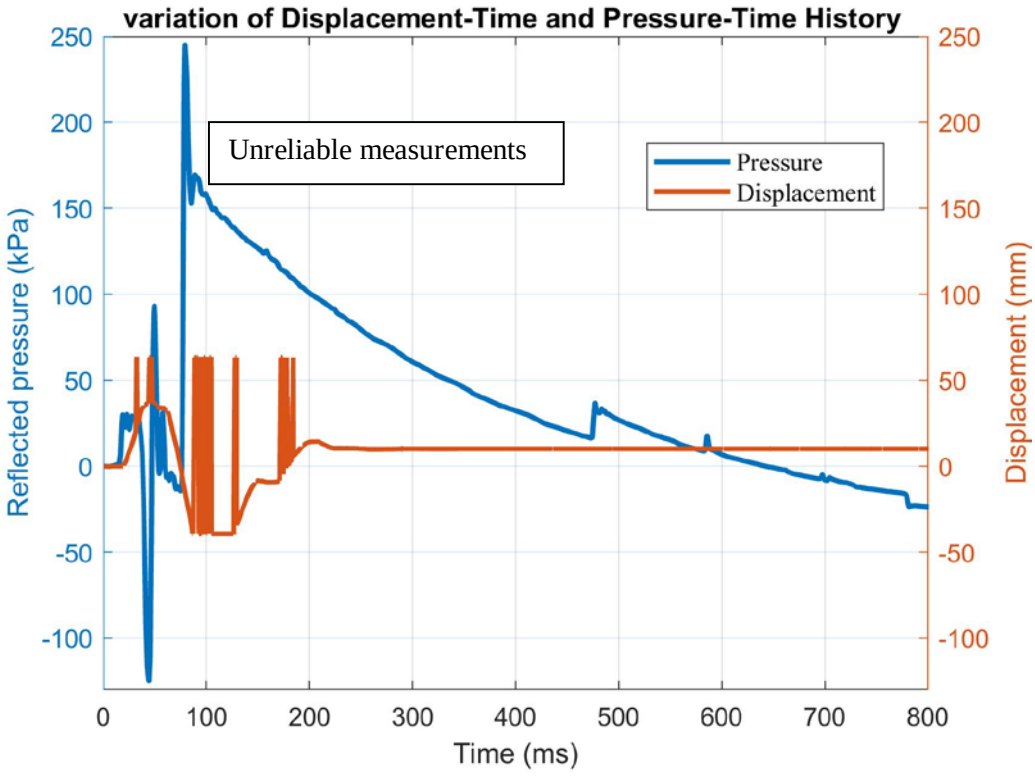

Figure A.25. Mid-span Panel Displacement and Pressure in Blast Test for JA-Plain-RF Test-2

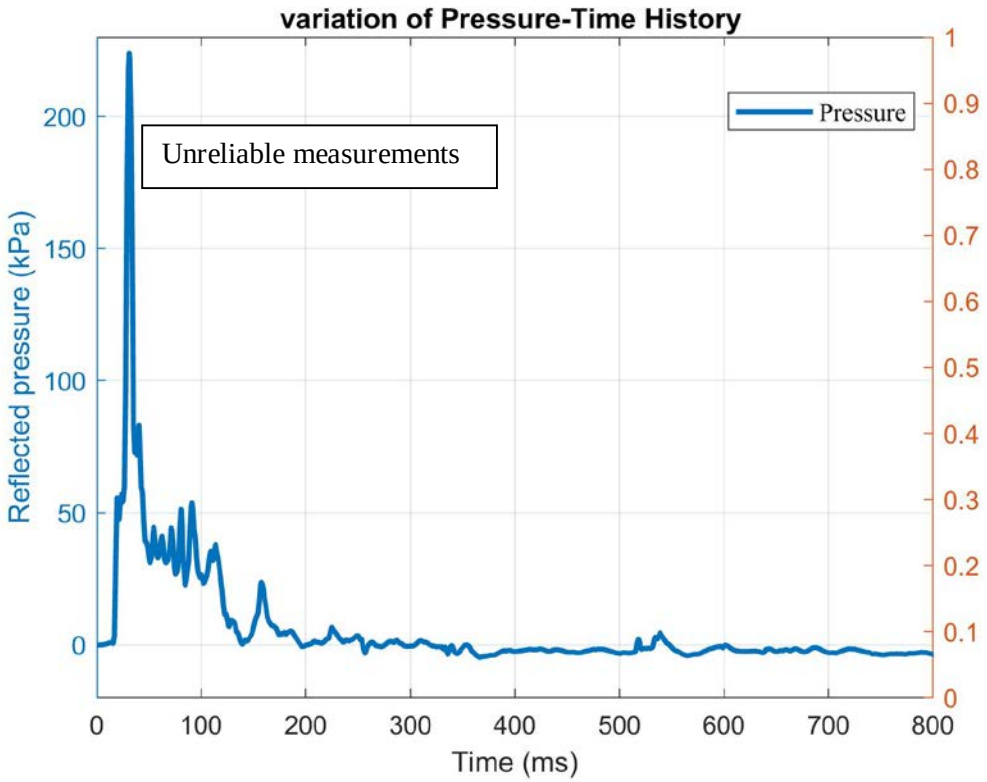

Figure A.26. Mid-span Panel Displacement and Pressure in Blast Test for JA-Plain-RF Test-3